The coupled stratospheric chemistry climate model LMDz-REPROBUS: description and evaluation of a transient simulation of the period 1980-1999.

L. Jourdain[1,3], S. Bekki[1], F. Lott[2], F. Lefèvre[1].

[1]Service d'Aéronomie, Université Paris 6, CNRS, 4 place jussieu, 75005, Paris France

[2]Laboratoire de Météorologie Dynamique, Université Paris 6, CNRS, 4 place jussieu, 75005, Paris France

[3]Now at the Jet Propulsion Laboratory, 4800 Oak Grove Dr., 91109 Pasadena, CA. USA.

Correspondence to : Line Jourdain (line.jourdain@jpl.nasa.gov)

Abstract

In order to study stratosphere-climate interactions, the stratospheric version of the General Circulation Model (GCM) LMDz, has been coupled interactively to a detailed stratospheric chemistry module (the same module as in the REPROBUS stratospheric chemistry transport model). In this paper, we present an extensive evaluation of the chemical and dynamical climatology of the stratosphere predicted by this new Chemistry-Climate Model (CCM). The simulation evaluated here is transient and covers the period 1980-1999. It takes into account the evolution of (i) the greenhouse gazes concentrations, (ii) the SSTs at the surface, and (iii) the halogen and aerosols loading of the stratosphere.

This CCM simulation does not present drifts. It has a dynamical climatology that is reminiscent of the climatology of the stratospheric version of the GCM LMDz, where ozone concentration fields are specified via climatologies. The introduction of an interactive stratospheric chemistry improves the model climatology, with a substantial reduction of the temperature biases in the low tropical stratosphere. However, at high latitudes in the Southern Hemisphere, there is a cold temperature bias that is much more pronounced than in the non-interactive version. It results from an amplification by the Chemistry of a moderate temperature error that is already present in the non-interactive version. It follows that in the CCM, the South Pole is much too isolated, which favours very low Antarctic Ozone values. As a consequence, the cold bias is amplified, maintaining low temperatures in the vortex, delaying its break-up and the recovery of Antarctic ozone later in the year.

The overall transport and chemical composition in the stratosphere are well simulated by the model. For instance, the latitudinal and vertical variation of the mean age of air compares reasonably well to the estimates derived from measurements, though the

model mean age of air is 1-3 years too young in the middle stratosphere. The model also reproduces the observed 'tape recorder' in tropical total hydrogen (=H_2O+2xCH_4), but its propagation is about 30 % too fast and its signal fades away slightly too quickly. The analysis of the global distributions of CH_4 and N_2O shows that the subtropical transport barriers are correctly represented in the simulation.

The spatial and seasonal variations of ozone are in very good agreement with ozonesondes in the low and middle stratosphere. The model reproduces also most of the large-scale features of the distributions of HNO_3, HCl revealed by the satellite measurements. The chemical polar processes and the contrast between the 2 hemispheres are reasonably well simulated during the winter. However, because of the cold bias, large discrepancies are found for most species at high latitudes in the Southern Hemisphere during the spring and early summer. In the Northern Hemisphere, polar ozone depletion and its variability are underestimated.

1. Introduction

Climate change and stratospheric ozone are coupled issues (World Meteorological Organisation/United Nations Environment Program (WMO/UNEP), 2007). Climate changes affect the dynamical structure and the chemical composition of the stratosphere in various ways through changes in the tropospheric wave forcing and through in situ changes in the radiative and chemical processes. In return, the stratosphere might play a more significant and complex role in tropospheric dynamics and climate than previously thought. Recent studies have indicated that middle and upper stratospheric dynamical perturbations may significantly influence the troposphere. In particular, strong correlation between the strength of the stratospheric polar vortex and the Arctic Oscillation, the dominant pattern of surface weather variability in the extratropics of the Northern Hemisphere, has been found in meteorological analyses with an apparent downward propagation of stratospheric circulation anomalies to the troposphere (Baldwin and Dunkerton, 2001). In the Southern hemisphere, stratospheric ozone depletion has contributed to increase the strength of the midlatitudes tropospheric winds and decrease the temperature over the Antarctic continent (WMO, 2007). Furthermore, stratospheric ozone also exerts a major influence on the chemical composition of the troposphere through chemically-driven mechanisms. For example, the flux of ozone coming from the stratosphere represents a major term in the tropospheric ozone budget (Karlsldottir et al., 2000; IPCC 2001) and stratospheric ozone levels are a determining factor in the amount of UV radiation reaching the troposphere and driving its chemistry (Madronich and Granier, 1992). As a result, stratospheric ozone perturbations can affect the oxidation efficiency of the troposphere and hence the levels of greenhouse gases such as tropospheric ozone and methane (Bekki et al., 1994). Finally, this influence of the stratosphere onto the troposphere has implications for understanding external climate forcing agents, such as the solar variability or volcanic eruptions that perturb directly the dynamics and chemistry of the stratosphere. Indeed, as discussed above, stratospheric perturbations may propagate to the troposphere through a mix of radiative, chemical and dynamical mechanisms. Quantifying the impact of theses natural forcings on the climate with respect to anthropogenic forcings is an important issue in climate change assessments.

The study of the interactions between climate change and stratospheric ozone requires the use of Chemistry-Climate Models (CCMs) (Austin et al., 2003; Eyring et al., 2006). A CCM is usually composed of a General Circulation Model (GCM)

coupled to a chemistry module. The model-calculated concentrations of radiatively species are used as input in the radiation code, allowing the chemical, radiative and dynamics processes to fully interact.

The purpose of this paper is to present the reference evaluation of the stratospheric CCM LMDz-REPROBUS that is part of the IPSL Earth system model. The atmospheric component of the Earth System model has been extended vertically to cover the domain of the stratosphere (Lott et al., 2005) and then coupled interactively with a stratospheric chemistry module. The simulated stratosphere of this coupled model is compared against a range of observations in order to evaluate the qualities and deficiencies of the model. This overall thorough evaluation is a necessary step before using the model for specific sensitivity studies or coupling to the rest of the Earth system model. Note that this model has also been intercompared with other CCMs in the framework of Eyring et al. (2006). So we present here a more detailed description and evaluation of our model.

The plan of the paper is as follows. Section 2 presents the model and the experimental set-up. In section 3, the climatological performances of the model regarding dynamics, transport and chemistry are evaluated from comparisons with meteorological analysis and observations. The results are summarized and discussed in section 4.

2. Model description and simulations

The dynamical model used is the extended version of the LMDz fourth-generation atmospheric GCM described in Lott et al. (2005). Its performances in the stratosphere and with a fixed ozone climatology are described in this paper, where a particular emphasis given to the simulation of the midlatitudes variability. An evaluation of its tropospheric climatology can also be found in Lott (1999) for the midlatitudes, and in Li (1999) for the tropics. Its tropospheric version is largely used in the French Research community (Hourdin et al., 2005, Bony et al., 2004, Quaas et al., 2004, Reddy and Boucher 2004, among others) and starts to include interactive tropospheric chemistry (Hauglustaine et al., 2004). This model is also the atmospheric component of the IPSL Earth System model (Dufresne et al., 2002).

It is a gridpoint model. In the horizontal direction, the equations are discretized on a staggered latitude-longitude Arakawa-C grid. It currently uses a uniform resolution of 2.5° in latitude and 3.75° in longitude. In the vertical direction, the discretization is in term of an hybrid sigma pressure vertical coordinate, where the

model level pressure $Pn=An+Bn*P/Ps$**.** It currently uses 50 levels, and the *Bn* values are near *0* above the log-pressure altitude of 13km, ensuring pure pressure vertical coordinates in the stratosphere. The *An* values are such that the upper level is near 65km, that the resolution in the stratosphere varies slowly from 1km at z=12km to 3km at z=50km and reaches 6km at the model top.

The salient features of the physical parameterizations used in the model are: a radiation scheme based on the ECMWF scheme (Morcrette 1989), a convection scheme based on Tiedtke (1989), a Subgrid Scale Orography (SSO, which forces orographic gravity waves) scheme based on Lott and Miller (1997) and Lott (1999), and a Doppler-spread non-orographic gravity waves scheme based on Hines (1997a, b) and adapted from Manzini et al. (1997). Note that compared to the stratospheric version in Lott et al. (2005), the parameter β of the SSO scheme that controls the amount of mountain gravity waves that propagate toward the middle atmosphere have been slightly modified. It is now equal to β=0.8 (instead of β=0.9): there are twice more mountain gravity waves reaching the stratosphere. This change was needed for our model to have a warmer Stratospheric North Pole in winter. Otherwise, the slightly two cold North Pole Temperature found in Lott et al. 2005 (see their Figure 13) induces far too much PSC and Ozone destruction by Heterogeneous Chemistry. Note also that the stratospheric version of LMDz also includes a Rayleigh drag sponge layer between 55km and 65km that damps the resolved waves and not the mean-flow (Shepherd et al., 1996).

The transport of tracers is calculated using the Van Leer scheme I (a first-order volume finite scheme with slope limitation) (Van Leer, 1977; Hourdin and Armengaud, 1999).

The chemistry model is the chemistry module of the REPROBUS (Reactive Processes Ruling the Ozone Budget in the Stratosphere) chemistry-transport model (Lefèvre et al., 1994, 1998). The chemistry model contains a detailed description of Ox, NOx, HOx, ClOx, BrOx and CHOx chemistry. It calculates the chemical evolution of 55 species using 160 gas-phase reactions and 6 heterogeneous reactions on sulphuric acid aerosols and PSCs. Reaction rates coefficients are taken from the recommendations of Sander et al. (2003). The photolysis rates are calculated at every time step using a look-up table from the Tropospheric and Ultraviolet visible (TUV) model (Madronich and Flocke, 1998) tabulated for 81 altitudes, 7 total ozone columns and 27 solar zenith angles. In the model, heterogeneous reactions take place on liquid binary (H_2O/H_2SO_4) and ternary ($H_2O/H_2SO_4/HNO_3$) aerosols as well as on

solid NAT or ice particles. The aerosol scheme (Carslaw et al., 1995) that simulates the surface and the composition of liquid aerosols assumes instantaneous thermodynamic equilibrium between the aerosol phase and the gas-phase (no kinetic barrier to condensation/evaporation and phase transition). Therefore, for example, ice particles form on NAT particles once the ice point is reached. The irreversible vertical transfer of HNO_3 and H_2O due to the sedimentation of PSCs (i.e. denitrification) is also taken into account.

In this study, we have performed a transient simulation of the period 1975-2000 using the CCM. The dynamical tendencies are evaluated every 3 minutes, the tracers advection and the chemical tendencies are evaluated every 15 minutes, the physical processes are evaluated every 30 minutes, except for the radiation transfer calculations that evaluated every 2 hours only. In order to save computing time, the model chemistry is only integrated above the level 13 (~ 400 hPa). Below this level, the chemical composition of the CCM is forced with a transient simulation from a global 2-D model.

The 2-D model is a global 2-D chemistry-transport-aerosol model extending from the ground to 60 km that is fully interactive in the stratosphere (Bekki an Pyle, 1992; Jones et al., 1995)). The model contains a detailed description of Ox, NOx, HOx, ClOx, BrOx, CHOx, and SOx photochemistry that is very similar to the CCM description. It uses recommended photochemical data (Sanders et al., 2003). It also includes a full microphysical aerosol scheme that allows to simulate the impact of volcanic eruptions on the stratospheric aerosol layer (Bekki and Pyle, 1994). The 2-D model is integrated from 1958 to 2000 with the temporal evolution of the mixing ratios of source gases (CO_2, CH_4, N_2O CFC11, CFC12, minor CFCs, HFCs, CH_3Cl, CH_3Br, Halons) prescribed at the surface on a monthly basis according to a standard WMO scenario (WMO, 1998). The effects of the volcanic eruptions of Agung in 1963, El Chichon in 1983 and Mount Pinatubo in 1991 are simulated by injecting 7, 10 and 20 MT of SO_2 in the tropics.

The forcing of the CCM chemical composition with the 2-D fields below 400 hPa acts as a sink in the CCM for NOy, inorganic chlorine Cly and inorganic bromine Bry and as a stratospheric source for CH_4, N_2O, organic chlorine (CFC11, CFC12, CFC113, CCl_4, CH_3CCL_3, CH_3Cl, HCFC22) and bromine (CH_3Br , Ha1211, Ha1301). Above 400 hPa, the evolution of stratospheric Cly and Bry levels in response to the increase in CFCs and halons concentrations is explicitly calculated in the CCM. The time-varying distribution of stratospheric sulphuric acid aerosols is

also provided by the 2-D model ensuring that the chemical effects of enhanced aerosol loading following large volcanic eruptions is taken into account in the CCM simulation.

The CCM is initialised in 1975 with the 2-D model fields. The mean amount of Cly and Bry in the stratosphere in 1975 is 1.2 ppbv and 10 pptv respectively. The CCM is fully interactive, that is the model-calculated fields of water vapor, ozone, CH_4, N_2O, CFC11 and CFC12 are used as inputs in the radiation transfer calculations. CO_2 mixing ratios used in the radiation transfer code are from the 2D model. Monthly mean sea surface temperatures are prescribed according to the AMIP2 data for the period 1975-2000 (Taylor et al., 2000). We will only present and analyse the last 20 years of our simulation corresponding to the 1980-1999 period, the first five years being used as spin-up.

3. Results

3.1 Dynamics

To validate the dynamical performances of our model, we will mainly use 20-years (1981-2000) of the ERA40 ECMWF analysis (Simmons and Gibson 2000).

3.1.1 Zonal mean Temperature

In this section, monthly mean temperature fields for the last 20-year of the simulation are presented for the four cardinal months January, April, July, and October. Figure 1 shows the zonal mean temperature from the model. It shows a well-defined mid-latitude tropopause around 10km, and a temperature minimum in the vertical around 16km in the tropics, a local temperature minimum in the winter polar lower stratosphere, and a well defined stratopause around 50km. At this level, the temperature is maximal in the vertical for all latitudes and seasons, and the pole to pole meridional temperature gradient reverses during solstice seasons, presenting a local maximum at the summertime polar stratopause.

Although these features agree qualitatively with the observations, some pronounced model biases can be seen, when compared with the ECMWF reanalysis in Figure 2. There is a warm bias around 5-10K near everywhere at the stratopause. The polar winter stratosphere is typically 5-10 K too cold in the SH, but slightly too warm in the Northern Hemisphere. In October, the Southern Hemisphere polar stratosphere is again 10-20 K too cold. Note that contrary to Lott et al. (2005), this simulation does not present a warm bias at the tropical tropopause, which is a clear

indication that this bias was probably due to the specification of the Ozone climatology, not to a problem of the model dynamics or of its radiation code.

3.2.2 Stratospheric planetary waves and polar Temperature

Most of the stratospheric variability in the Northern Hemisphere arises from large-scale perturbations of the polar vortex by upward propagating planetary waves that originate in the troposphere (Charney and Drazin, 1961). Accordingly, a good representation of these planetary waves is essential for our stratospheric climate to be reasonable. The January statistics of the first 3 planetary waves from the model are shown in Figure 3. The corresponding fields from the reanalysis are shown in Figure 4. Overall, it is clear that the rather realistic simulations of the zonal mean fields and tropospheric climate result in the forcing of planetary waves that are both realistic in phase and amplitude. Note nevertheless that the model has a tendency to underestimate the amplitude and variability of the first 3 planetary waves in the Northern Hemisphere. It is interesting to notice here that those results are opposite to those in Lott et al. (2005) who found that the Stratospheric version of LMDz tends to slightly overestimate the Planetary Waves (PWs) in the Northern Hemisphere winter. Sensitivity tests done over a shorter period than that documented here, suggest that this is due to the change in the SSO parameter β described in the Section 2. This change yields to a more realistic zonal mean Temperature, but also yields to a smaller planetary wave variability. Note nevertheless that the model now overestimates the Northern polar temperature by 5 K in winter. The general tendency for the model to underestimate the PWs variability is also found in the Southern Hemisphere (not shown). As the PWs were a little overestimated in the Southern Hemisphere as well in Lott et al. (2005) we found here a sensitivity to the subgrid scale mountain gravity waves that we did not expected (there are much less mountains in the Southern Hemisphere than in the Northern Hemisphere).

The Figure 5 shows time series of the simulated mid-stratosphere temperatures over the poles. The model captures the general nature of the temperature variations, their seasonal dependence and the contrasts between the two hemispheres that can be seen in Figure 6 for the ECMWF reanalysis. However, the model has a slight warm bias of near 5K at the North Pole and a pronounced cold bias of near 10 K in SH late winter and early spring. In addition, the model Northern Hemisphere polar temperature displays greater interannual variability from February to April (late winter to early spring) than does the reanalysis. The North Pole time series also show

that the model develops shorter lasting warmings than in the reanalysis. The interannual variability in the timing also shows that the warmings in the model happen only once at the end of December, in contradiction with the reanalysis, where those are more frequent in mid-December. Figure 6 also shows that the warmings in the model occur throughout the winter, and that the vortex can reconstruct after a warming simulated between January and February. The variability in the South Pole temperature at 10 hPa is realistic as well, with the difference between the years much smaller than for the North Pole. The South Pole time series shows no significant warming.

Although the LMDz-REPROBUS simulation is in generally good agreement with ERA 40 reanalysis, the Southern hemisphere suffers from the common cold pole bias: the polar vortex is too strong and persists too long during the year until early summer. This bias is more pronounced than in Lott et al. (2005) where ozone concentration fields are specified via climatologies. Accordingly, we attribute the strong cold bias in the Southern Hemisphere Temperature at the pole to a retroaction of the chemistry. This will be illustrated in section 3.3.

3.2 Transport

In this Section**,** we present conventional diagnostics of the transport in our simulation.

3.2.1 Mean age of air

To calculate the mean age of the air in the stratosphere, we follow Hall and Prather (1993) and include in the model an inert tracer whose concentration grows linearly with time below a given lower boundary. In the present study, this boundary is the equatorial tropopause between 15°N and 15°S and the mean age of air at a given point in the stratosphere is derived from the difference between the mixing ratio of this tracer at that point and its mixing ratio at the tropical tropopause. The time lag is calculated after 20 years of simulation.

Figure 7a shows the zonally and annually averaged mean age in our simulation. In it, we see that the isopleths of the mean age bulge upward in the tropics and slope downward to the poles as a result of the Brewer-Dobson meridional circulation. The quasi-horizontal mixing by the planetary scale wave "breaking" is also clearly apparent in the flattening of the isopleths at midlatitudes (see Figure 7a).

In Figures 7b-e, the annually averaged mean age of air in the simulation is

evaluated more thoroughly by comparison with estimates from the SF6 and CO2 observations reported by Hall et al. (1999). The Figure 7b shows that in the low stratosphere the model reproduces very well the latitudinal distribution of the mean age of air. The vertical profile of the mean age of air in the tropics (Figure 7c) is also well reproduced, but the air is a year too young above 22 km. As reported by Waugh and Hall (2002), several factors could contribute to decrease the mean age of air in this region as a too rapid meridional circulation, a too weak mixing with midlatitudes air or too much vertical diffusion (explicit or numerical). We have not performed model sensitivity studies to theses different aspects of the transport. This limits our ability to draw definitive conclusions on the reasons of the discrepancies. However, we can note that the model appears to reproduce the shift between the tropical and the extratropical profiles of the mean age of air (Figures 7c and 7d respectively) as well as the steep latitudinal gradient of the mean age in the lower stratosphere (Figure 7b), suggesting a correct isolation of the tropics in our simulation. This aspect is further investigated later on.

At middle and high Northern latitudes in the low stratosphere, (Figures 7d and 7e respectively) the model age of air increases with altitude in agreement with the observations. Note that this increase is the result of the quasi-horizontal wave-driven mixing, because the transport by the mean residual circulation alone would tend to produce the highest values of the age of air in the lower stratosphere at high latitudes (Waugh and Hall, 2002). On the contrary, the model simulates a pronounced maximum in the polar lower stratosphere in the Southern Hemisphere, consistent with the weaker quasi-horizontal mixing in this hemisphere (Figure 7a). Again, the model nevertheless underestimates the mean age of air at high latitudes of the Northern Hemisphere above 25 km. This discrepancy is particularly pronounced inside the polar vortex (Figure 7e), where observations indicate values greater than 7 (instead of 4 years in our simulation).

Overall, although the air tends to be too young by 1 to 3 years in the middle and upper stratosphere, the model does reproduce the latitudinal and vertical variation of the mean age of air reasonably well. The transport in our model is found to be more realistic than in most of the models evaluated within the framework of the Models and Measurements II project presented in Hall et al. (1999) (see Figures 7b-d) and is comparable with the state of Arts CCMs presented in Eyring et al. [2006].

3.2.2 Tape recorder signal

The seasonal temperature changes at the equatorial tropopause induce a seasonal variation of the water vapor entering into the lower tropical stratosphere. The vertical propagation of this water vapor seasonal cycle is the "tape recorder" (Mote et al., 1995,1996). The analysis of this signal provides informations on the ascent rate and on the diffusion in the tropical upwelling as well as on the intensity of the mixing with the extratropical air. In the following, we use the variable part of the total hydrogen $\hat{H}$= 2 CH_4+ H_2O, that is better conserved than water vapor (John et al., 1986), to analyse the tape recorder signal in the model.

Figure 8 presents the model-calculated $\hat{H}$ mixing ratios averaged between 12 N and 12 S as a function of altitude and time. The model reproduces the typical seasonal variation of $\hat{H}$ at the equatorial tropopause with a minimum during boreal winter and a maximum during boreal summer. In order to determine the variation of the amplitude (A) and the phase lag (τ) of the tape recorder propagation, the simulated $\hat{H}$ profiles (Figure 8) are fitted to the function,

$$X(z,t) = A(z) \cos(\omega(t - \tau(z)),$$

using the Levenberg-Marquardt least square fit algorithm. The amplitude is assumed to decay exponentially with the altitude : $A(z) = A_o e^{-z/H_a}$, with A_o, the maximum amplitude of the signal and H_a the decay scale height, indicating of the attenuation rate of the tape recorder with altitude. The ascension rate c is supposed to be constant, giving a phase lag $\tau(z)=z/c$. In Figure 8, our results are also compared with estimates derived from the analysis of $\hat{H}$ observations from the Halogen Occultation Experiment (HALOE) instrument on the Upper Atmospheric Research Satellite (UARS) by Mote et al. (1998) and from in situ aircraft and balloon measurements of CO_2 and $\hat{H}$ reported in Hall et al. (1999). Note that in order to compare model and observations, we normalized the amplitude to unity at a reference level (Figure 8), which corresponds to the level of the maximum amplitude for the model (ie : 17 km) and to 16 km for the observations as in Hall et al. (1999). The phase lag τ is also taken null at this reference level.

The model slightly underestimates the phase lag in the low stratosphere, it equals 0.6 years at z-zref=8 km whereas the analyses of Mote et al. (1998) and Randell et al. (1998) of the HALOE data give 0.8 years and of 0.9 years respectively at the same level. The model mean ascent rate over the first 10 km of the lower stratosphere is about 0.44 mm/s, which is higher than the corresponding value of 0.3 mm/s estimated by Mote et al. (1998). Figure 8 also suggests that the model

overestimates slightly the attenuation of the amplitude A with the altitude. The decay scale height Ha of the amplitude is found to be about 3.7 km.

Overall, the results indicate that the model tends to propagate the tape recorder too fast (by about 30 %), which is consistent with our underestimation of the age of air in the tropics (Figure 7c). The model also tends to attenuate slightly too much the amplitude of the tape recorder. This latter discrepancy could be due to too much mixing between extratropics and tropics but this problem was not revealed by our analysis of the mean age of air distribution (see Section 3.2.1.). This discrepancy could also be due to too much vertical diffusion in the upwelling (in our case numerical diffusion due too the transport scheme, the explicit diffusion occurring only in the boundary layer in the model). This could explain as well the too young mean age of air in the tropics. However, as noted by Hall et al. [1999] and Waugh and Hall [2002], it is difficult to sort out the reasons of the discrepancies without performing sensitivities studies to the different aspects of the transport.

3.2.3 Long- lived species

In this part, we examine the CCM's distribution of CH_4 and N_2O. The top 4 panels in Figure 9 shows the January, April, July and October zonal mean distributions of CH_4 simulated by the LMDz-REPROBUS model for the 1991-1997 period. The lower 4 panels in Figure 9 show the corresponding values derived from the Halogen Occultation Experiment (HALOE) and the Cryogenic Limb Array Etalon Spectrometer (CLAES) on the Upper Atmospheric Research Satellite (UARS). The HALOE data (version 18) covers the period November 1991-March 1997 and have been combined with CLAES data obtained between January 1992 and March 1993 in the polar regions (Randell et al., 1998). This climatology is available on the SPARC Data Center (http://www.sparc.sunysb.edu/).

For the 4 months in Figure 9, the model reproduces correctly the zonal mean distribution of CH_4. In the winter hemisphere and below 10mb, the steep latitudinal gradients in the subtropics and in the polar regions are well reproduced. In midlatitudes, the flattening of the contours due to the quasi horizontal mixing by the planetary waves breaking in the surf zone is also correctly reproduced. Still in those Figures but for the summer hemisphere, the isopleths are less steep in the subtropics and they gradually flatten out at high latitudes, again as in the HALOE-CLAES

climatology. The model also produces an equatorial double peak during the equinox above 1 mb altitude. As in the observations, these peaks are particularly pronounced in Northern Hemisphere spring. Nevertheless, they are less pronounced in the model than they are in the HALOE observation below 1mb. Although this defect is common to many models (Kennaugh et al., 1997) it is probably natural here, in the sense that our model does not have a QBO, so the zonal winds in the tropical lower stratosphere are always easterlies. This is consistent with Kennaugh et al. (1997) and Randel et al. (1997) who found that the double peak in the CH_4 observations is weak or even inexistent when the phase of the QBO correspond to easterlies. This comparison also shows that the model underestimates the CH_4 mixing ratios in July at high latitudes in the Southern Hemisphere, confirming the too strong isolation of the vortex. Because the vortex persists too long in the Southern Hemisphere, as noticed previously in Figure 5, the model still underestimates the CH_4 mixing ratios in this region in early summer (January).

In order to investigate further the isolation of the tropical regions in the model, we have also evaluated the position and extent of the subtropical boundary in the model following Sparling et al. (2000) and Neu et al. (2003). Figure 10 shows the latitudinal distribution of N_2O mixing ratios at 15 hPa for August 1990-1999 and the corresponding area-weighted probability density functions (PDFs) of N_2O mixing ratios at this level in the Northern and Southern Hemisphere. N_2O mixing ratios are binned on 5 ppbv intervals and the PDFs are smoothed with a 5 ppbv running average. The Northern and Southern Hemispheres are separated according to the latitude of the tropical maximum. This Figure 10 can be compared to the PDFs of N_2O mixing ratios obtained with CLAES observations for August 1992 by Sparling et al. (2000) (see their Figure 3). The peaks in the distribution reveal the presence of three distinct air masses in the winter hemisphere (Southern Hemisphere) corresponding to the tropics, the midlatitudes surfzone, and the polar vortex, and two distinct air masses in the summer hemisphere (Northern Hemisphere) corresponding to the tropics and the extratropics. The minima of the distribution correspond to the transition regions between the different types of air masses. We focus here on the subtropical transition regions. We have calculated for each hemisphere and for each year the PDFs of the latitude corresponding to N_2O values in the subtropical transition regions, using the same approach than Neu et al. (2003). We define the latitude of the subtropical boundary as the most probable latitude and we interpret the width of the distribution as a measure of the extent of the transition regions following

Neu et al. (2003).

For the winter hemisphere, we find that the subtropical transition region is very narrow and that the most probable position of the subtropical barrier at 15 hPa ranges between 11.25 S and 13.75 S depending on the year. For the summer hemisphere, the subtropical transition region is very large from 8.75-13.75 N to 33.75-43.75 N depending on the year. These results are comparable with those derived from the analysis of the CLAES and HALOE observations [Sparling et al., 2001; Neu et al., 2003]. Note that we could not determine a value for the summer subtropical boundary as the transition is gradual in our simulation. However, the position center of the subtropical region is comparable with the position of the subtropical barrier in the studies cited above. Overall, this shows that the model correctly reproduces the positions and the extents of the subtropical transition regions in the middle stratosphere.

3.3. Distributions of chemically reactive species

3.3.1 Ozone

The vertical and seasonal variation of ozone mixing ratios in the stratosphere have been evaluated using a climatology which combines HALOE and Microwave Limb Sounder (MLS) satellite data (Randel et al., 1998) and in situ measurements over several ozonesondes stations from the World Ozone and Ultraviolet Radiation Data Centre (WOUDC) for the period 1986-1995. Figure 11 shows that the model reproduces correctly the maximum of about 10 ppmv near 10 hPa in the tropics, as well as its slight seasonal shift toward the summer hemisphere. However, there are differences with the observations regarding the shape of the isopleths in the winter hemisphere. In January, the slope of the ozone isopleths, downward from the equator to the pole, in the lower stratosphere is steeper in the model than in the observations. In the southern hemisphere extratropics, the sharp decrease of the ozone mixing ratios with decreasing latitude confirms the too strong isolation of the vortex.

The comparison with the ozonesondes measurements in Figure 12 shows that the model reproduces very well the magnitude of the O_3 mixing ratios as well as its seasonal cycle in the lower and middle stratosphere. At middle and high latitudes, the maximum in the middle stratosphere (10 hPa) in the summer hemisphere (due to the chemistry) and the spring maximum in the lower stratosphere (at 40 hPa and 90 hPa) (that is due to the transport) are reproduced. The model overestimates the ozone mixing ratios in the middle and lower stratosphere in the Southern Hemisphere

midlatitudes (Lauder, 45S). This discrepancy is consistent with the reduced transport from middle to high latitudes in this hemisphere due to the strong isolation of the vortex. Over Syowa (69S), the model underestimates the ozone concentrations at 40 hPa in spring. This results again from the cold bias at high latitudes in the Southern Hemisphere, leading to excessive PSC formation and subsequent ozone destruction. We can also note that the model tends to overestimate the ozone mixing ratios in the lowermost stratosphere over Alert (82N) and Hohenpeissenberg (48N). This discrepancy results from a slightly too strong transport from the region of production. In the tropics, the magnitude and the weak seasonal cycle of ozone mixing ratios are well reproduced.

The seasonal variation of the Total Ozone Column has also be examined by comparing the modeled values with the merged TOMS/SBUV dataset (http://code916.gsfc.nasa.gov/Dataservices/merged/mod_data.public.htlm) for the period 1990-2000 (Figure 13). In the Northern Hemisphere, the main features of the annual cycle of total ozone with a maximum during the winter/spring season and a minimum during the summer/autumn are correctly captured by the model. The total ozone minima in the tropics and the weak seasonal cycle are also correctly reproduced. However, the total ozone values in the tropics are somewhat overestimated by up to about 40 DU. As the agreement with tropical ozonesondes is satisfactory in the lower and middle stratosphere, this discrepancy is in fact due to an overestimation of the tropospheric ozone column. This problem originates from the difficulty in maintaining the strong vertical gradients of ozone in the tropopause region. It is important to note that since the model is relaxed below 400 mbar toward the 2D model ozone fields, this problem has a significant impact only in the tropical and subtropical regions, where the tropopause is situated well above 400 mbar all the year around. In these regions, the ozone amount between 400 mbar and the tropopause increases during the simulation. Indeed, tropospheric ozone columns of 50 DU are simulated on average in the tropics for the last year of the simulation (not shown) which is too high. In the Southern Hemisphere, the model simulates the development of the Antarctic ozone hole in spring. However, the model simulates a deeper ozone hole: observations indicate a monthly mean value of 160 DU in October whereas the model calculates a mean value of 80 DU. The model also predicts a longer lasting ozone hole. This discrepancy is explained by the cold bias in the lower stratosphere over Antarctic in winter and spring in the model (see Figure 6), which contributes to low ozone values by enhancing polar ozone destruction. This

in turn contributes to maintain low polar temperatures and the vortex in spring and early summer. Most chemistry climate models suffer from this cold bias, albeit on a smaller scale (Eyring et al., 2006). The polar processes are investigated in more detail in the section 3.3.4.

3.3.2 HNO3

The Figure 14 presents the January and July zonal mean distributions of HNO_3 measured by CLAES between January 1992 and April 1993 (Kumer et al., 1996) and simulated by the model over the same period. The model reproduces correctly the latitudinal increase of HNO_3 from the equator to the pole as well as its vertical distribution. In both the observed and model-simulated distributions, the highest mixing ratios are found in the winter hemisphere, near the pole in the northern hemisphere, and at midlatitudes in the Southern Hemisphere. The magnitude of the simulated concentrations is also in good agreement with the measurements, except at high latitudes in the Southern Hemisphere lowermost stratosphere, where the cold bias leads to an overestimation of the denitrification (i.e. irreversible loss of HNO_3 by sedimentation of PSCs) in winter and spring compared to CLAES data. In particular, we can note that the denitrification seen by CLAES is not total, and is confined to altitudes below 30 hPa whereas it is already present at 15 hPa in the simulation. Because of the cold bias, the recovery of HNO_3 is also delayed in the model; this will be further discussed in the section dedicated to polar processes.

3.3.3 HCl

Figure 15 compares the zonally and monthly mean distribution of HCl observed by HALOE and simulated by the model. HCl along with $CLONO_2$ is the most important reservoir species for the inorganic chlorine family. In the upper stratosphere, the HCl mixing ratios is a measure of the total reactive chlorine available for the chemistry. In the polar lower stratosphere, it plays a key role in the heterogeneous chlorine activation processes. The HCl mixing ratios increase in the stratosphere with the altitude from 0.5 ppbv to about 3.5 ppbv in the mesosphere. The observations show also an increase of the HCl mixing ratios with the latitude. The model reproduces the overall distribution of HCl except at high latitudes in the Southern Hemisphere due to the cold bias. However, the model tends to overestimate the mixing ratio values compared to the HALOE data. The maximal difference is about 0.5 ppbv. From the previous analysis of the age of air and tape recorder signal,

we would expect an overestimation of the transport of the organic species in the upper stratosphere and hence an underestimation of the Cly (total inorganic chlorine) and HCl mixing ratios. However, the discrepancy could be related to the initialization of Cly in the stratosphere or/and to the too fast transport of HCl, which due to its relative long lifetime can be influenced by the transport.

3.3.4 Polar Ozone

PSCs Occurence

The Figure 16 shows the comparison between the area where the temperature is low enough for the formation of PSCs at 50 hPa (assuming 195 K for the PSC temperature threshold) during the winters 1990-1999 for both hemisphere in the model and in the ERA40 ECMWF reanalysis. Owing to the warm bias in the polar Northern Hemisphere in the model (See Figures and 6), the model largely underestimates the PSC area by a factor of about 2-3 over Arctic region and from January to March. It does not predict the presence of PSCs in December. The amount of PSCs interannual variability, an important features of the Northern Hemisphere, is also underestimated because the model simulates warm winters only. In the Southern Hemisphere, the PSCs area calculated during austral winter is in good agreement with estimates based on ERA40 but it is overestimated in October by almost 50 % due to the cold bias in this region. The complete disappearance of PSCs is delayed by about 8 weeks in the model and occurs in late December. The weak interannual variability of the magnitude of PSCs area over Antarctic is correctly reproduced by the model.

Polar ozone depletion processes for the Southern Hemisphere

Figure 17 presents an example of Southern Hemisphere polar temperature, N_2O, HNO_3, ClO, Chemical loss rates of ozone, O_3, $ClONO_2$, HCl distributions at 50 hPa during late winter and early spring (August 1, September 25, and October 15) for a typical year of the simulation in 1990s (corresponding to a 1993 forcing). The simulated gas-phase HNO_3 distribution presents a typical collar shape during winter with very low values (less than 0.5 ppbv) in the polar vortex and higher values of around 8 ppbv in the collar region. The simulated timing and magnitude of the decline in lower stratospheric gas-phase HNO_3 inside the vortex are in good agreement with the climatology derived from MLS observations by Santee et al. (1999) (not shown). However, the progressive recovery of the gas-phase HNO_3 observed by MLS in August when the temperatures rise is not simulated because

the denitrification is complete in our simulation which is not the case according to MLS data (Santee et al., 1999). As observed by Santee et al. (2003), enhanced ClO concentrations appear at the vortex edge in May in the model (not shown) and extend toward the pole during the course of winter. We calculate maximum daily-averaged values of 0.8 ppbv in late September, corresponding to a maximun daylight value of 1.6 ppbv. These enhanced values are also consistent with a nearly complete conversion of stratospheric chlorine to reactive forms. The ratio ClOx/Cly, where ClOx= Cl + ClO +2 Cl_2O_2 and Cly is the total inorganic chlorine, reaches a maximum of 96 % during this period. The Figure 17 shows that the large values of ClO inside the polar vortex are correlated with low values of HCl and $ClONO_2$. At the vortex edge, $ClONO_2$ forms the typical collar shape observed by CLAES (Roche et al. 1993). Ozone starts to be depleted at the edge of the vortex in August and is completely destroyed in the vortex core by mid October at 50 hPa. A maximal ozone chemical ozone loss rate of 0.1 ppmv/day is calculated at 50 hPa for late September. The monthly averaged ozone chemical loss rate in September in the vortex (75-90S) at 50 hPa is 0.09 ppmv/day which is in good agreement with ozone loss estimates derived from POAM II observations in 1994 , 1995 and 1996 (Hoffman et al., 1997). According to ClO observations (Santee et al., 2003; Solomon et al. 2002), chlorine deactivation occurs in mid and late September. In the simulation, this decline is delayed by a couple of weeks. As noticed in Douglass et al. (1995), ClO is mainly converted into HCl via the reaction Cl+CH_4 because the very low O_3 concentrations result into high Cl/ClO ratios and hence high Cl levels. However, note that, owing to the complete denitrification in the polar vortex, the decline of ClO is exclusively due to the reformation of HCl (via the reaction Cl+CH_4) with no contribution of the reaction CLO+NO_2.

The evolution of the simulated ozone in the polar vortex for the 1993 year has also been evaluated with the corresponding ozone soundings at the South Pole. We present in Figure 18 the comparison between the evolutions of observed and simulated ozone at different levels at South Pole. Figure 18 shows that the model reproduces correctly the rapid ozone decline between early September and early October as well as the magnitude of this decline below 30 hPa. However, the comparison at 20 hPa shows that the vertical extent of the ozone hole is overestimated by the model. This is due to the cold bias which extends to this altitude triggering large ozone depletion. In addition, the low temperatures persist too long in the model, delaying the ozone recovery in the lower stratosphere by 2-3 months, as

shown in Figure 18. Note that the overestimation of the ozone hole vertical extent can partly explain the delay in the vortex break-up as the warming occurs first in the middle stratosphere.

Polar ozone depletion in the Northern Hemisphere

Figure 19 presents an example of Northern Hemisphere HNO_3, ClO, Chemical loss rates of ozone, O_3, $ClONO_2$, HCl distributions at 50 hPa during late winter and early spring (January 15 , March 10, and March 30) for one of the coldest winter in our simulation (corresponding to a 1996 forcing). The magnitude and the spatial extent of ClO enhancement are smaller in the Northern Hemisphere than in the Southern Hemisphere (Figure 17), which is in agreement with observations. The denitrification is much weaker as well. As observed in the measurements, the main process leading to ClO deactivation in the Northern Hemisphere in the model is the reaction of ClO with NO_2 to reform $ClONO_2$. By the end of March, the cumulated ozone destruction reaches a maximum value of 0.7 ppmv at 60 hPa (not shown). This value can be compared with 1.65 ppmv +/- 20 % found for the winter 1999/2000 at 475 K which was one of the coldest winter of the 1990's and which was extensively studied (WMO, 2003). The small bias in temperature in the polar Northern Hemisphere leads to an important underestimation of the PSCs (Figure 16) and hence of the ozone depletion in our model. Overall, the main processes of the polar ozone depletion are correctly reproduced by the model. But, in the Southern hemisphere, the vertical extent of the ozone hole is overestimated and the recovery of the ozone hole is delayed. In the Northern hemisphere, the ozone depletion and its variability are underestimated because of a slight warm bias.

4. Conclusion

We have developed the LMDz-REPROBUS chemistry-climate model**,** which combines interactively a general circulation model and a stratospheric chemistry module. This paper has presented a detailed evaluation of a transient simulation covering the period 1980-1999 and taking into account the evolution of greenhouse gazes, of halogen and aerosols loadings in the stratosphere, and the SSTs at the surface. We find that this simulation does not present drifts and that the model is able to reproduce the most important physical and chemical processes in the stratosphere.

Concerning the dynamics, the model reproduces the vertical and zonal structure of the temperature as well as its seasonal variation. However, the model exhibits a slight warm bias of about 5 K in the Arctic polar lower stratosphere in winter and an elevated cold bias of about 10-20 K in the Antarctic polar lower stratosphere in late winter and spring. The comparison between Lott et al. (2005) and this study reveals a sensitivity of the model mean Northern Hemisphere polar temperature and variability to the amount of orographic waves entering the stratosphere. The bias in temperature in the Southern Hemisphere polar stratosphere is far more pronounced than in Lott et al. (2005) where ozone concentration fields are specified via climatologies. For this reason, we attribute this bias to an amplification of a moderate temperature error by a retroaction of the chemistry. The feedback of the chemistry is clearly apparent in our simulation. Indeed, because of the cold bias, the ozone depletion is overestimated by the CCM, in particular its vertical extent. This in turn contributes to maintain low polar temperatures in the vortex and delay the recovery of ozone and the break-up of the vortex.

We have evaluated the transport in the stratosphere in our model by examining the distributions of the mean age of air, CH_4 and N_2O as well as the propagation of the tape recorder signal. The model results are in reasonable agreement with observations and are also comparable to the State of the Art CCMs evaluated in Eyring et al. (2006). More specifically, the analysis of the latitudinal variation of the mean age of air and of the subtropical barriers suggests a correct isolation of the tropics in our model. However, the model tends to underestimate the age of air in this region by about 1 year and tends to propagate the tape recorder too rapidly by 30 %. This remains unexplained and could be related to shortcomings in the Brewer Dobson Circulation and/or too much vertical diffusion in the tropical upwelling due to some numerical diffusion. This latter possible deficiency could also explain the slightly too fast attenuation of the tape recorder in the model. However, to better

understand the reasons for these discrepancies, we would need to perform sensitivities studies to the different aspects of the transport, such as for example the advective scheme. In the midlatitudes and high latitudes, variations of the mean age of air and the distributions of the long lived species are well reproduced. This suggests that our model has a realistic balance between transport by the meridional circulation and by the quasi-horizontal mixing due to the planetary waves breaking. However, the magnitude of the mean age of air is well reproduced in the lower stratosphere in these regions but underestimated in the middle and upper stratosphere by about 1-3 years. This result was also found in Eyring et al. (2006) and needs further investigation. The evaluation of the distribution of the long-lived species also emphasizes the need to better represent the transport from the mesosphere to the upper stratosphere in winter in the model. A version of the model extended to the mesosphere is being developed. The diagnostics of the transport will be used to test the future versions of the model.

Most of the seasonal and spatial variations of chemical species are correctly reproduced in the model. In particular, the ozone field is in very good agreement with ozonesondes measurements at most altitudes in the low and middle stratosphere. The noticeable exception is in the Southern Hemisphere winter and spring, where the impact of the cold bias is clearly visible. However, the chemical polar processes and the contrast between the 2 hemispheres are reasonably well simulated during the winter. Finally, in order to address more accurately the interactions between atmospheric chemical composition and climate, the future model versions will also include tropospheric chemistry.

Figures

Figure 1 : Zonal mean Temperature from the last 20-year (1980-1999) of the LMDz-REPROBUS simulation. Contour interval=10K, values below 250K dashed.

Figure 2 : Same as Fig 1 but from the ECMWF reanalysis.

Figure 3: January Planetary waves diagnostics of geoptential height fields for 20 winters and from the LMDz-REPROBUS model. model. Wave with zonal wavenumber 1: a) mean amplitude, b) mean phase, and c) intra-seasonnal standard deviation due to wave 1. Wave with zonal wavenumber 2: d) mean amplitude, e) mean phase, and f) intra-seasonnal standard deviation due to wave 2; Wave with zonal wav/enumber 3: g) mean amplitude, h) mean phase, and i) intra-seasonnal standard deviation due to wave 3.

Figure 4 : Same as Fig 3 but from the ECMWF reanalysis

Figure 5 : Polar temperatures at 10hPa in LMDz and for 10 years (1980-1989) for (a) the northern hemisphere, and (b) the southern hemisphere.

Figure 6 : Same as Fig 7 but from the ECMWF reanalysis.

Figure 7: Annually and zonally averaged mean age of air relative to the equatorial tropopause and after 20-years of the LMDz-REPROBUS simulation(see text for details). (a) Latitude-altitude section, the dotted thick line indicates the thermal tropopause and the contour interval is 0.5 year.; (b) Latitudinal variation at the altitude z=20km. (c) vertical profile at the latitude 5S, (d) vertical profile at the latitude 40N, and (e) vertical profile at the latitude 65N. In b), c), d), and e) the solid line is for the model values while the various symbols are derived from observations: in situ CO2 (triangles) are from Boering et al. (1996) and Andrews et al. (2001b), in situ SF6 (diamonds) are from Elkins et al. (1999) Ray et al. (1999) and from SF6 whole-air samples are from Harnish et al. (1996) (asterix outside the vortex and crosses inside the vortex). See also Hall et al. (1999) for details on those measurements.

Figure 8: Variable part of the total hydrogen $\hat{H}$ (= $2CH_4 + H_2O$) simulated by the LMDz-REPROBUS and averaged over the Equatorial regions (12S-12N). Time altitude cross Section for the 1986-1995 anomaly (top). Equatorial profiles of the amplitude attenuation A (z) (bottom left) and the phase lag $\tau(z)$ (bottom right) of the tape recorder in the lower and middle troposphere derived from in situ CO2 (crosses), in situ $\hat{H}$ (stars) and HALOE $\hat{H}$ (dashed-dotted line) as reported in Hall et al. (1999) and from the analysis of the simulated anomalies field shown in the upper panel (solid black line). The altitude (zref) where the amplitude attenuation and the

phase lag are equal to 1 and 0 respectively is at 16 km for the observations and for the model it corresponds to the level of maximum amplitude of the signal.

Figure 9: January, April, July and October zonal mean distributions of CH4 simulated by the model for the period 1990-1999 (top) and observed by HALOE and CLAES (bottom).

Figure 10: Latitudinal distribution of the simulated N2O mixing ratios at 15 hPa in August for 1990-99 (top left). Area weighted PDF of the N2O mixing ratios for the winter hemisphere (top right) and for the summer hemisphere (bottom left). PDF of the latitude of the subtropical boundary region (bottom right, see text for definition) for the winter and summer hemispheres for each year from 1990 (blue) to 1999 (red).

Figure 11: January and July zonal mean distributions of O3 mixing ratios (ppmv) simulated by the model for the period 1990-1999 (top) and observed by HALOE and MLS (bottom).

Figure 12: Seasonal variation of O3 mixing ratios (ppmv) over different stations measured by sondes and simulated by the model. Measurements (black dots) and simulated mixing ratios (open squares) are averaged over the period 1986-1995. Note that the standard deviation for the model is not shown as for practical reasons we archived 5-day average outputs for most of the years of simulation.

Figure 13: Variation of total ozone (in Dobson unit) with latitude and time (month); top panel: mean value for the last 10 years of the simulation (1990-1999), bottom panel: mean value of TOMS/SBUV observations for the period 1990-1999.

Figure 14: January and July zonal mean distributions of HNO3 mixing ratios (ppbv) simulated by the model for the period 1990-1999 (top) and observed by CLAES (bottom).

Figure 15: January and July zonal mean distributions of HCL mixing ratios (ppbv) simulated by the model for the period 1990-1999 (top) and observed by HALOE (bottom).

Figure 16: Fractions of the Northern hemisphere area (right) and of the Southern hemisphere (left) covered by PSCs (with temperature below 195 K) at 50 hPa calculated by ERA 40 (top) and simulated by the model (bottom) for the period 1990-1999.

Figure 17: Distribution of the temperature (K), N2O (ppbv), HNO3 (ppbv), ClO (ppbv), chemical loss rate of ozone (ppbv/day), O3 (ppmv), ClONO2 (ppbv), HCl (ppbv) over Antarctic at 50 hPa between late winter and early spring (August 1, September 25, and October 15) for the year corresponding to the 1993 forcing.

Figure 18: Evolution of the measured and simulated ozone mixing ratios at South Pole at 10, 20, 30, 50 and 90 hPa during 1993.

Figure 19 : Distribution of HNO3 (ppbv), ClO (ppbv), chemical loss rate of ozone (ppbv/day), O3 (ppmv), ClONO2 (ppbv), HCl (ppbv) over Arctic at 50 hPa between winter and spring (January 15, March 10, and March 30) for the year corresponding to the 1996.

References

Austin et al., Uncertainties and assessments of chemistry-climate models of the stratosphere, *Atmos. Chem. Phys*., 3, 1-27, 2003.

Baldwin M. P. and Timothy J. Dunkerton, Stratospheric Harbingers of Anomalous Weather Regimes, *Science* 294 (5542), 581-584, 2001.

Bekki S., J. Pyle Two-Dimensional Assessment of the Impact of Aircraft Sulphur Emissions on the Stratospheric Sulphate Aerosol Layer, *J. Geophys. Res.*, V. 97, D14, 15839-15847, 1992

Bekki, S., J. A. Pyle, A two-dimensional modeling study of the volcanic eruption of Mount Pinatubo, J. Geophys. Res., 99(D9), 18861-18870, 10.1029/94JD00667, 1994.

Bekki, S., K. S. Law, J. A. Pyle, Effect of ozone depletion on atmospheric CH4 and CO concentrations, *Nature,* 371, 595-597, 1994.

Bony S, Dufresne J-L, LeTreut H, Morcrette J-J, Senior C, On dynamic and thermodynamic components of cloud changes. *Climate Dynamics* 22: 71-86, 2004.

Carslaw K. S. et al., An analytic expression for the composition of aqueous HNO_3-H_2SO_4 stratospheric aerosols including gas phase removal of HNO_3. *Geophys. Res. Lett., 22*, 1877-1880, 1995.

Charney J.G., Drazin P. G. (1961) Propagation of planetary-scale disturbances from the lower into the upper atmosphere. *J Geophys Res* 66: 83-109.

Dufresne et al., On the magnitude of positive feedback between future climate change and the carbon cycle, *Geophys. Res. Lett.*, 29, 1405, doi : 101029/2001GL013777.

Hall, T.M., and M.J. Prather, 1993: Simulations of the trend and annual cycle in stratospheric CO_2. *J. Geophys. Res.*, **98**, 10573-10581, doi:10.1029/93JD00325.

Hall T. M., D. W. Waugh, K, A. Boering and R. A. Plumb, Evaluation of transport in stratospheric models, *J. Geophys. Res.* , 104, 18815-18839, 1999.

Hauglustaine et al., Interactive photochemistry in the Laboratotoire de Météorologie Dynamique general circulation model : Description and background tropospheric chemistry evaluation , *J. Geophys. Res.*, 109, D04314, doi; 10.1029/2003JD003957, 2004.

Eyring, V., et al. (2006), Assessment of temperature, trace species, and ozone in chemistry-climate model simulations of the recent past, *J. Geophys. Res.*, *111*, D22308, doi:10.1029/2006JD007327

Hines, C.O., Doppler spread parameterization of gravity wave momentum deposition in the middle atmosphere. Part 1 : Basic Formulation, J. *Atmos. Sol. Terr. Phys., 59*, 371-386, 1997a.

Hourdin F. and A. Armengaud, The use of finite-volume methods for atmospheric advection trace species: 1. Tests of various formulations in a general circulation model, *Mon. Weather Rev*., 127, 822-837, 1999.

Hourdin, F., I. Musat, S. Bony, P. Braconnot, F. Codron, J.-L. Dufresne, L. Fairhead, M.-A. Filiberti, P. Friedlingstein, J.-Y. Grandpeix, G. Krinner, P. Levan, and F. Lott, The LMDZ4 general circulation model: climate performance and sensitivity to parametrized physics with emphasis on tropical convection, *Climate Dynamics*, 27, DOI:10.1007/s00382-006-0158-0,2006.

Jones, R.L., J.A. Pyle, J.E. Harries, A.M. Zavody, J.M. Russell III, and J.C. Gille, The water vapour budget of the stratosphere studied using LIMS and SAMS satellite data, Q. J. R. Meteorol. Soc., 112, 1127-1143, 1986.

Jones, A.E., S. Bekki, and J.A. Pyle,On the atmospheric impact of launching the Ariane-5 rocket, *J. Geophys. Res.*, 100, 16651-16660, 1995.

Karlsdottir, S., I. S. A. Isaksen, G. Myhre, Trend analysis of O3 and CO in the period 1980-1996:A three-dimensional model study, *J. Geophys. Res.*, 105, 28907-28993, 2000.

Lefèvre et al., Chemistry of the 1991/1992 stratospheric winter: Three dimensional model simulations, *J. Geophys. Res*., 99, 8183-8195, 1994.

Lefèvre, F., F. Figarol, K. S. Carslaw, T. Peter, The 1997 Arctic ozone depletion quantified from three-dimensional model simulations, *Geophys. Res. Lett.*, 25(13), 2425-2428, 10.1029/98GL51812, 1998.

Li L. (1999) Ensemble Atmospheric GCM simulation of climate interannual variability from 1979 to 1994. *J Climate* 12: 986-1001.

Lott F., Alleviation of stationary biases in a GCM through a mountain drag parameterization and a simple representation of mountain lift forces, *Mon. Weather Rev*.127, 788-801, 1999.

Lott F. and M. Miller, A new subgrid scale orographic drag parameterization; its testing in the ECMWF model, *Quaterly Journal of the Royal Meteorological Society*, 123, 101-127, 1997.

.Lott, F.,L. Fairhead, F. Hourdin and P. Levan, The stratospheric version of LMDz: Dynamical Climatologies, Arctic Oscillation, and Impact on the Surface Climate. *Climate Dynamics, 25,* 851 – 868. DOI: 10.1007/s00382-005-0064-x

Kennaugh R.,S. Ruth and L. Gray, Modeling quasi-biennal variability in the semiannual double peak, *J. Geophys. Res.,* 102, 16169-16187, 1997.

Madronich, S., and C. Granier, Impact of recent total ozone changes on tropospheric ozone photodissociation, hydroxyl radicals, and methane trends, *Geophys. Res. Lett.*, 19, 465-467, 1992.

Madronich, S. and S. Flocke, The role of solar radiation in atmospheric chemistry, *Handbook of Environmental Chemistry (P. Boule, ed.)*, Springer-Verlag, Heidelberg, pp. 1-26,1998

Manzini et al., Impact of the Doppler spread parameterization on the simulation of the middle atmosphere circulation using the MA/ECHAM4 general circulation model, *J. Geophys. Res*., 102, 25751-25762, 1997.

Manzini E, McFarlane NA (1998) The effect of varying the source spectrum of a gravity wave parameterization in a middle atmosphere general circulation model. *J Geophys Res* 103: 31,523-31,539.

Morcrette, J.-J., Description of the radiative scheme in the ECMWF model, *Technical Report, N\260165*, ECMWF, Reading, United Kingdom, 26. pp, 1989.

Mote, P. W., K. H. Rosenlof, J.R. Holton, R. S. Harwood and Joe Waters, Seasonal variations of water vapor in the tropical lower stratosphere, Geophys. Res. Lett., 1093-1096, 1995.

Mote P. W et al., An atmospheric tape recorder : the imprint of tropical tropopause temperatures on stratospheric water vapor, *J. Geophys. Res.,* 101, 3989-4006, 1996.

Mote P. W., T. J. Dunkerton, M. E. McIntyre, E. A. Ray, P. H. Haynes and James M. Russell III, Vertical velocity, vertical diffusion, and dilution by midlatitude air in the tropical lower stratosphere, *J. Geophys. Res*., 103, 8651-8666, 1998.

Neu J. L., L.C. Sparling an R. A. Plumb, Variability of the subtropical "edges" in the stratosphere, *J. Geophys. Res.,* 108, doi: 10.1029/2002JD002706, 2003.

Quaas J., Boucher O., Bréon F.-M. (2004) Aerosol indirect effects in polder satellite data and the laboratoire de meteorologie dynamique-zoom (lmdz) general circulation model. *J Geophys Res* 109: D08205, doi: 10.1029/2003JD004317.

Randel, W.J., Wu, F., Russell, J.M.,III, Roche, A., and J.W. Waters, Seasonal cycles and QBO variations in stratospheric CH_4 and H_2O observed in UARS HALOE data, *J. Atmos. Sci, 55*, 163-185, 1998.

Randel, W. J.III, J. Waters, Space-time patterns of trends in stratospheric constituents derived from UARS measurements, *J. Geophys. Res.*, 104(D3), 3711-3728, 10.1029/1998JD100044, 1999

Rayner, et al., Version 2.2 of the global sea-ice and sea-surface temperature dataset, 1903-1994, *CRTN 74, Hadley Centre, Meteorol. Off. Bracknell, U. K.,* 1996.

Reddy M. S., Boucher O. (2004) A study of the global cycle of carbonaceous aerosols in the lmdzt general circulation model, *J Geophys Res* 109: D14202, doi:10.1029/2003JD004048.

Rozanov E.V., M. E. Schlesinger, V. A. Zubov, The University of Illinois, Urbana-Champaign three-dimensional stratosphere-troposphere general circulation model with interactive ozone photochemistry : Fifteen-year control run climatology, *J. Geophys. Res.*, 106,1-22, 2001.

Sadourny and Laval, January and July performance of the LMD general circulation model, in New Perspectives in Climate Modelling, *edited by A. Bergerand C. Nicolis, pp. 173-198, Elsevier Sci., New York*, 1984.

Santee, M. L. et al., UARS Microwave Limb Sounder HNO_3 observations: Implications for Antarctic polar stratospheric clouds, *J. Geophys. Res., 103*, 13285-13313, 1998

Shepherd et al. Sponge layer feedbacks in middle atmosphere models, *J. Geophys. Res.*, 101, 23447-23464, 1996.

Simmons A. J., Gibson JK (2000) The ERA-40 project plan. ERA-40 Project Report Series 1: 63p.

Sparling L. C., Statistical perspectives on stratospheric transport, *Rev. Geoph.*, 38, 417-436, 2000.

Steil B., C. Bruhl, E. Manzini, P. J. Crutzen, J. Lelieveld, P. J. Rash, E. Roeckner and K. Kruger, A new interactive chemistry-climate model: 1. Present-day climatology and interannual varibility of the middle atmosphere using the model and 9 years of HALOE/UARS data, *J. Geophys. Res.*, 108, doi:10,1029/2002JD002971, 2003.

Taylor K. E., D. Williamson, and Francis Zwiers, the Sea surface Temperature and sea-ice concentration boundary concentrations for AMIP II simulations, *PMCDI Report 60, Program for Climate Model Diagnosis and Intercomparison, Lawrence Livermore National Laboratory*, 2000.

Tiedtke, M., A comprehensive mass flux scheme for cumulus parameterization in large scale models, Mon. Weather Rev., 117, 1779-1800, 1989.

Van Leer B.. Towards the ultimate conservative difference scheme. IV. A new approach to numerical convection, *J. Comput. Phys.*, 23, 1977.

Waugh D. W. and T. M. Hall, Age of stratospheric air: theory, observations and models, *Rev. Geophys*., 40, doi:101029/2002RG000101, 2002.

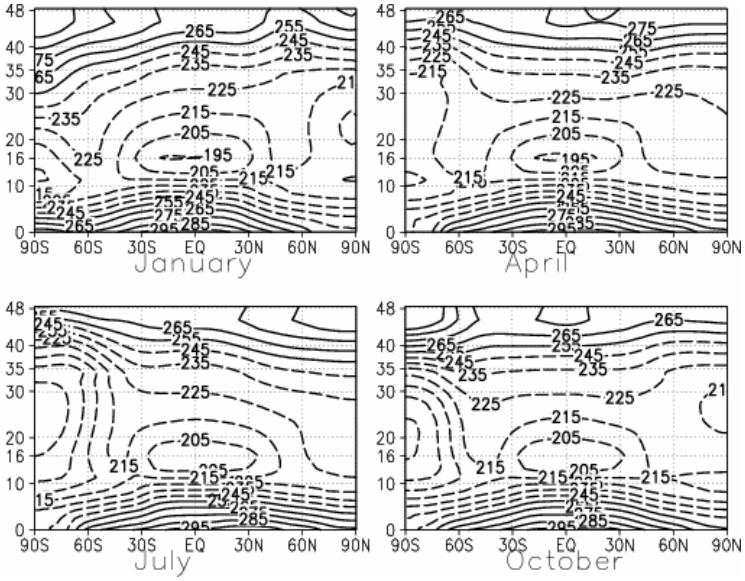

Fig 1: Zonally averaged temperature fields in Kelvin, calculated from a 20-year run with the LMDz model. Contour interval=10K, values below 250K dashed.

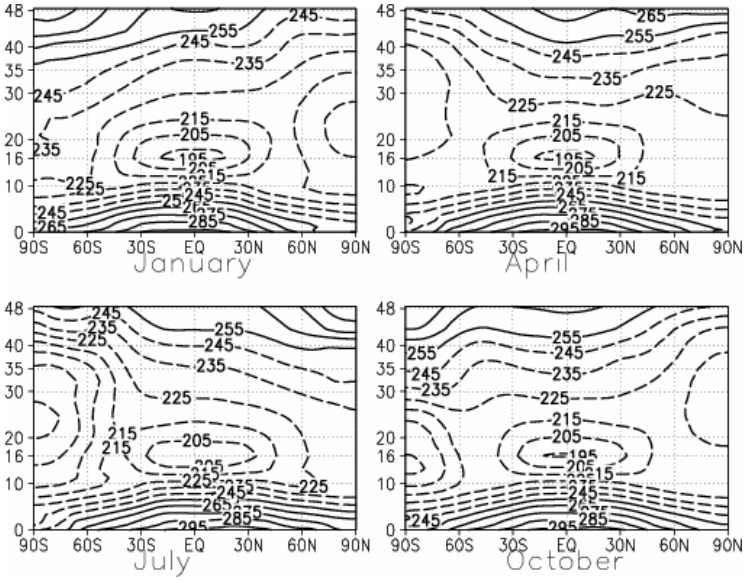

Fig 2: Same as Fig 1 but from the ECMWF climatology.

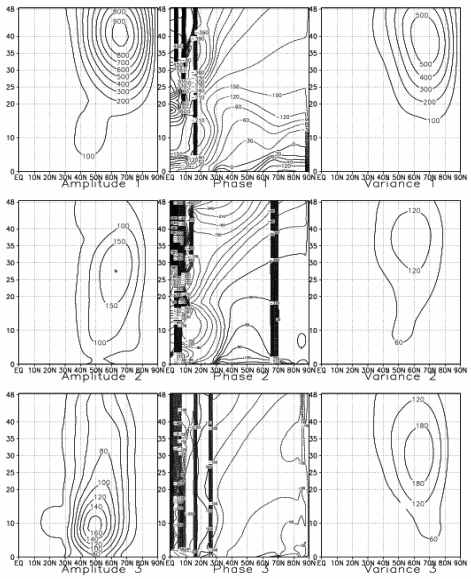

Fig 3: January Planetary waves diagnostics of geoptential height fields for 20 winters and from the LMDz model. Wave with zonal wavenumber 1: a) mean amplitude, b) mean phase, and c) intra-seasonnal standard deviation due to wave 1. Wave with zonal wavenumber 2: d) mean amplitude, e) mean phase, and f) intra-seasonnal standard deviation due to wave 2; Wave with zonal wavenumber 3: g) mean amplitude, h) mean phase, and i) intra-seasonnal standard deviation due to wave 3.

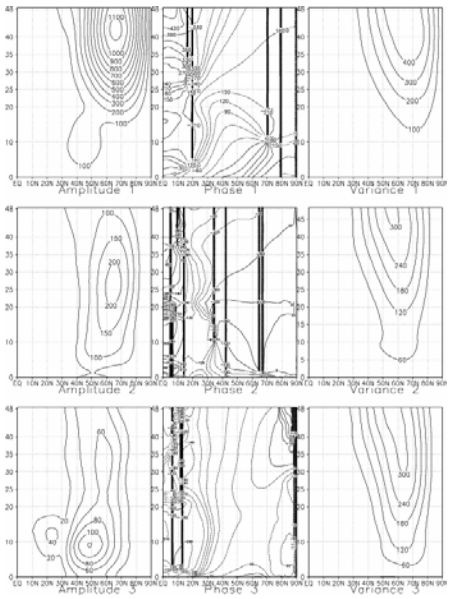

Fig 4: Same as Fig 3 but for the ECMWF reanalysis.

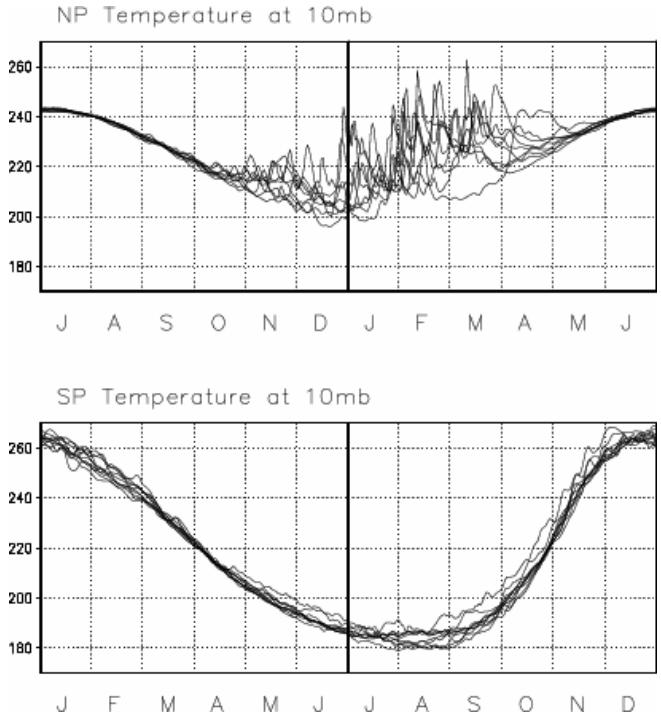

Fig 5: Polar temperatures at 10hPa in LMDz and for 10 years (1980-1989) for (a) the northern hemisphere, and (b) the southern hemisphere.

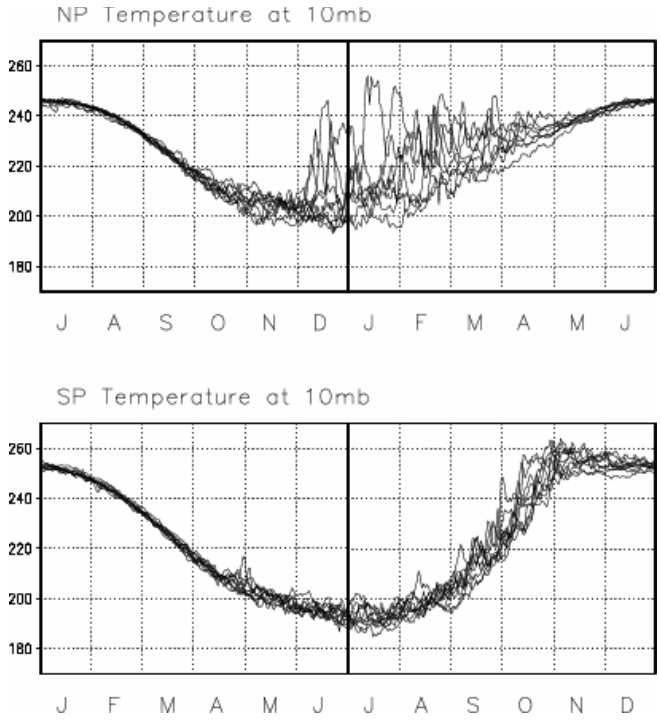

Fig 6 : Same as Fig 7 but for the ECMWF reanalysis.

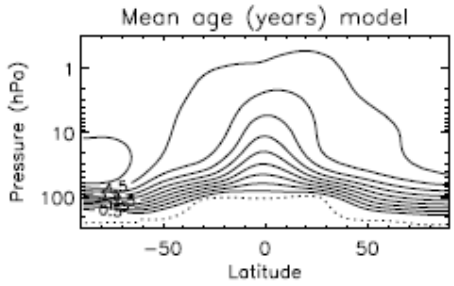

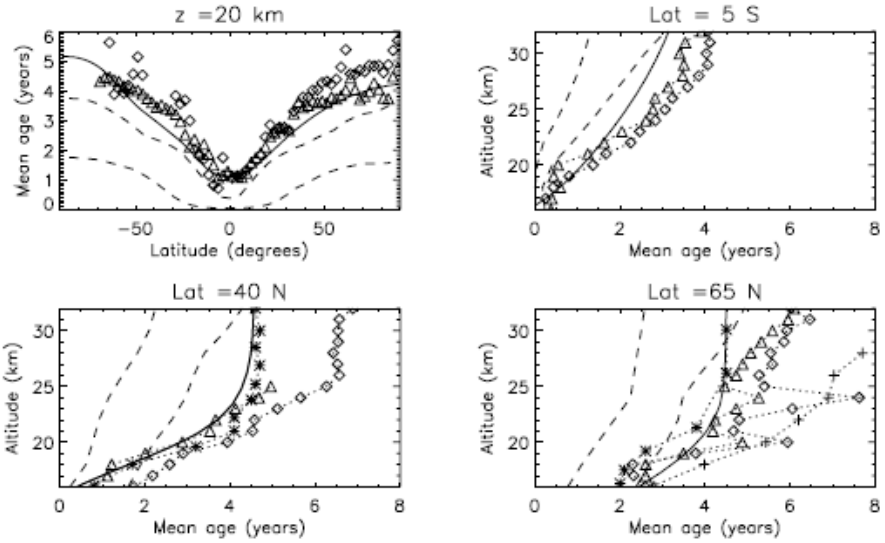

Figure 7: Annually and zonally averaged mean age of air relative to the equatorial tropopause and after 20-years of the LMDz-REPROBUS simulation (see text for details). (a) Latitude-altitude section, the dotted thick line indicates the thermal tropopause and the contour interval is 0.5 year.; (b) Latitudinal variation at the altitude z=20km. (c) vertical profile at the latitude 5S, (d) vertical profile at the latitude 40N, and (e) vertical profile at the latitude 65N. In b), c), d), and e) the solid line is for the model values while the various symbols are derived from observations: in situ CO2 (triangles) are from Boering et al. (1996) and Andrews et al. (2001b), in situ SF6 (diamonds) are from Elkins et al. (1999), Ray et al. (1999) and SF6 whole-air samples are from Harnish et al. (1996) (asterix outside the vortex and crosses inside the vortex). See also Hall et al. (1999) for details on those measurements.

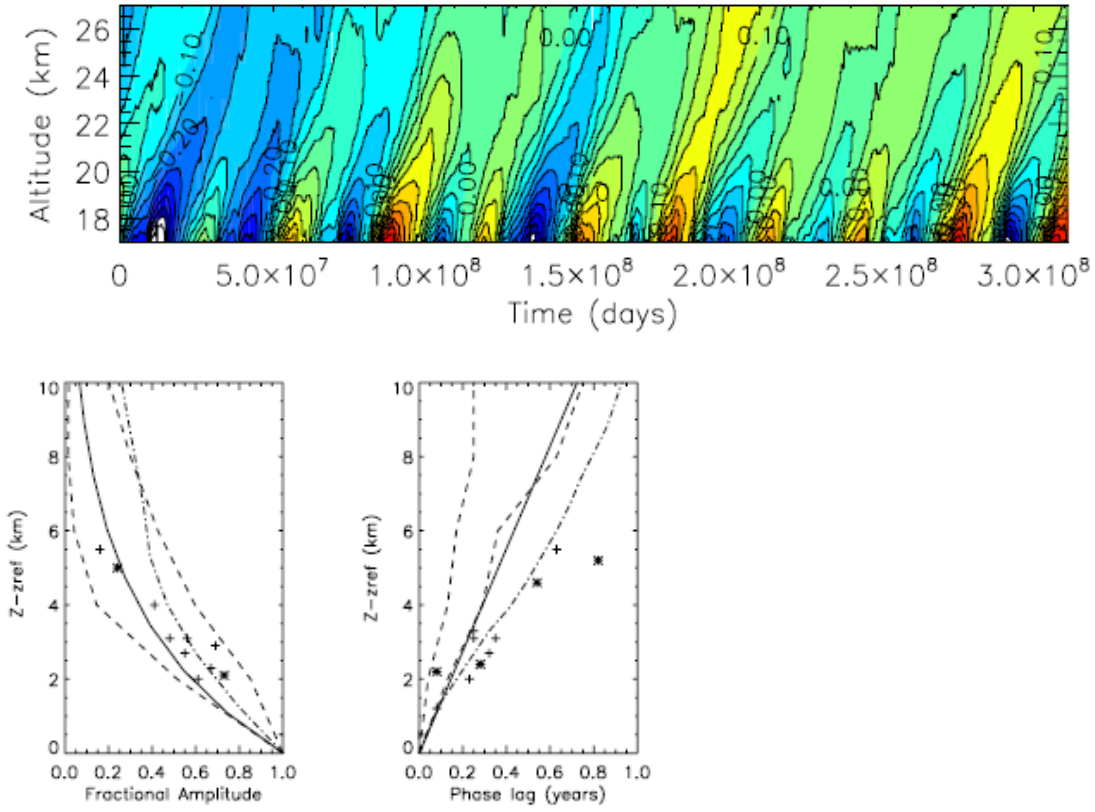

Figure 8: Variable part of total hydrogen $\hat{H}$ (= $2CH_4$ + H_2O) simulated by the LMDz-REPROBUS and averaged over the Equatorial regions (12S-12N). Time altitude cross section for the 1986-1995 anomaly in LMDz-REPROBUS (ppmv) (top). Equatorial profiles of the amplitude attenuation A (z) (bottom left) and the phase lag $\tau(z)$ (bottom right) of the tape recorder in the lower and middle troposphere derived from in situ CO2 (crosses), in situ $\hat{H}$ (stars) and HALOE $\hat{H}$ (dashed-dotted line) as reported in Hall et al. (1999) and from the analysis of the simulated $\hat{H}$ anomalies field shown in the upper panel (solid black line). The altitude (zref) where the amplitude attenuation and the phase lag are equal to 1 and 0 respectively is at 16 km for the observations and for the model it corresponds to the level of maximum amplitude of the signal.

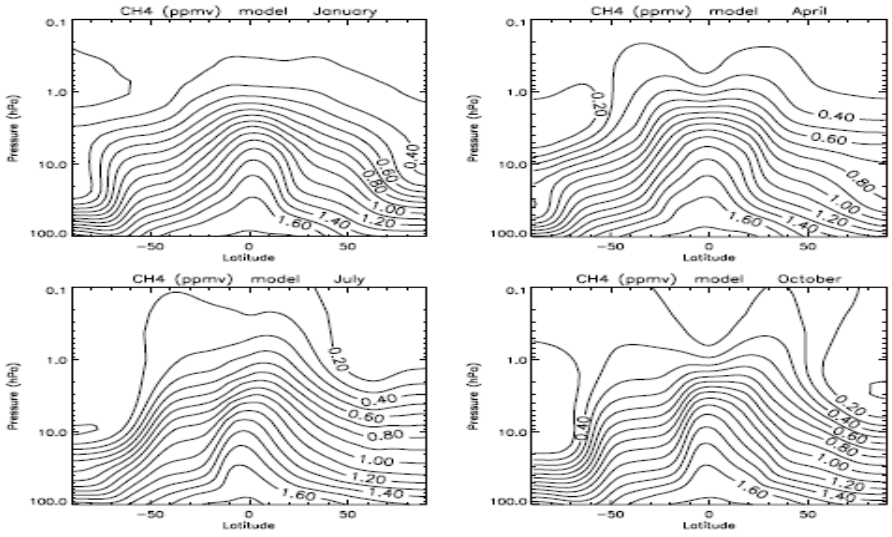

1

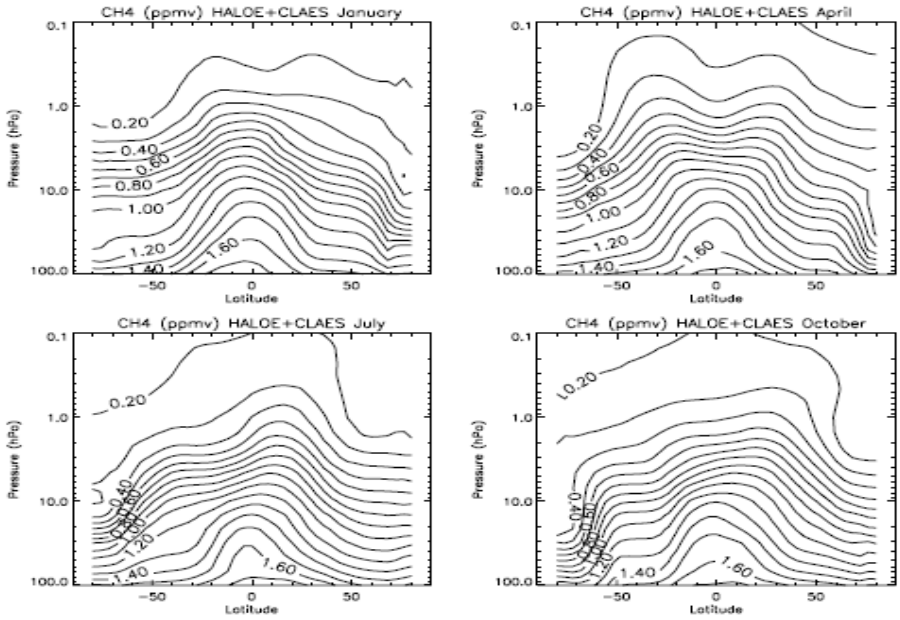

2

3

4 **Figure 9:** January, April, July and October zonal mean distributions of CH4
5 simulated by the model for the period 1990-1999 (top) and observed by HALOE and
6 CLAES (below).

7

8

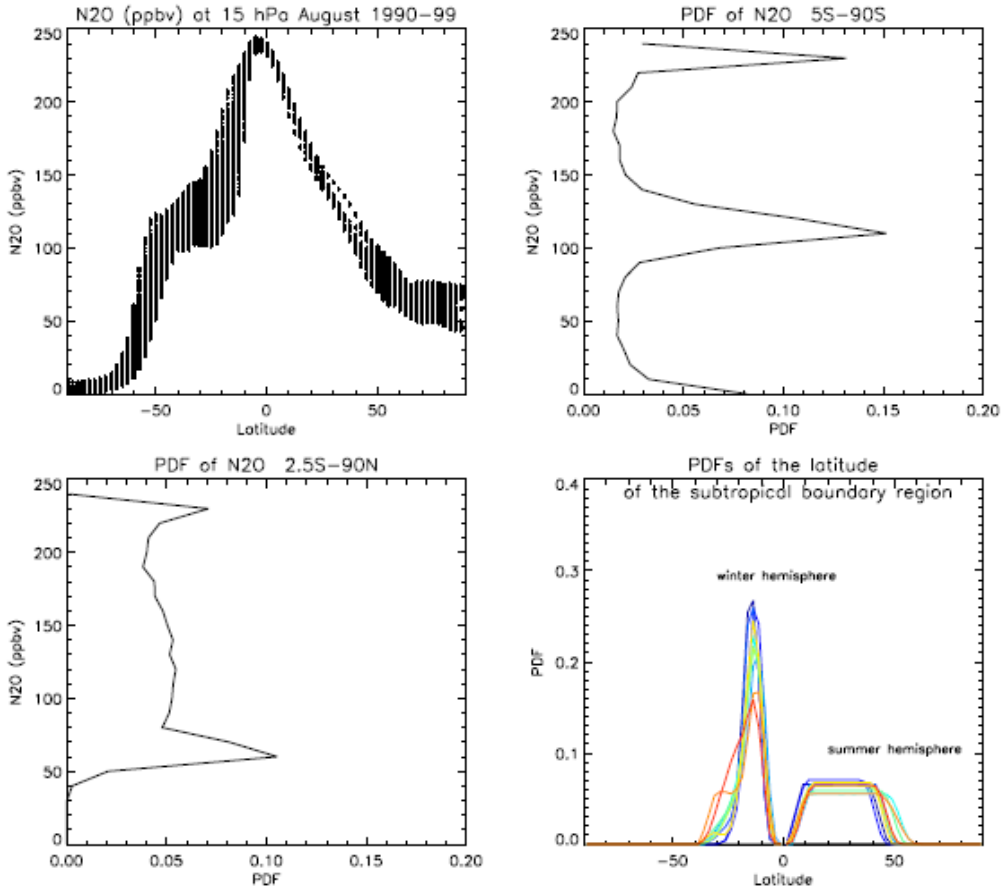

Figure 10: Latitudinal distribution of the simulated N2O mixing ratios at 15 hPa in August for 1990-99 (top left). Area weighted PDF of the N2O mixing ratios for the winter hemisphere (top right) and for the summer hemisphere (bottom left). PDF of the latitude of the subtropical boundary region (bottom right) for the winter and summer hemispheres for each year from 1990 (blue) to 1999 (red).

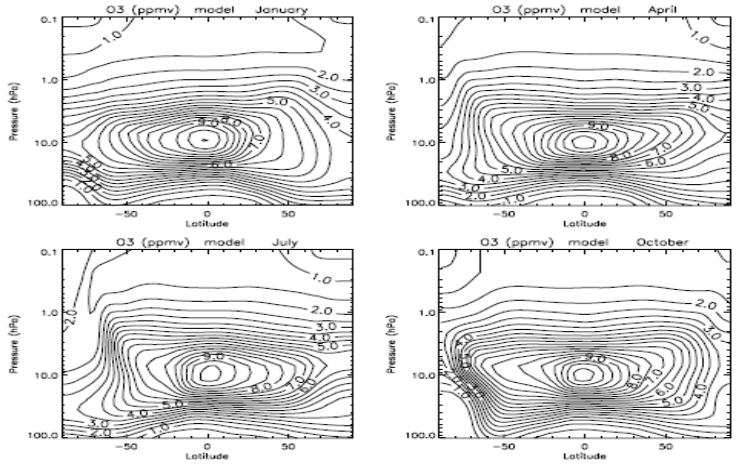

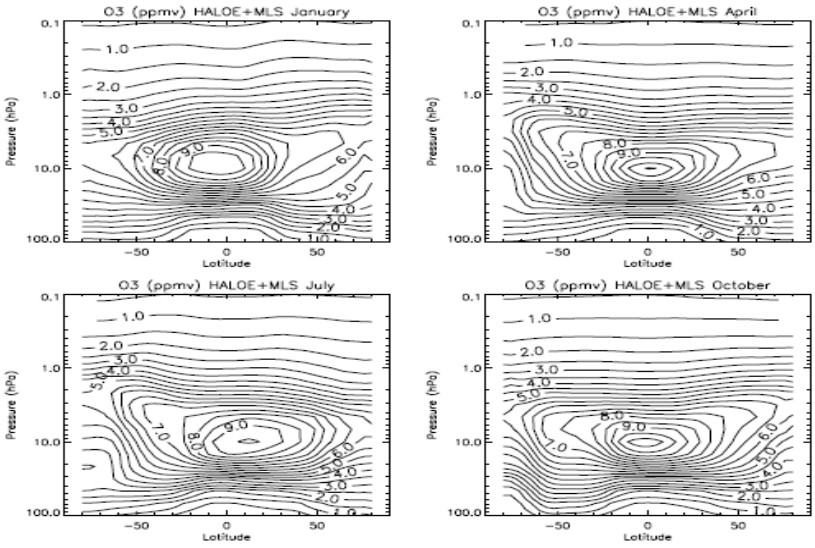

Figure 11: January and July zonal mean distributions of O3 mixing ratios (ppmv) simulated by the model for the period 1990-1999 (top) and observed by HALOE and MLS (below).

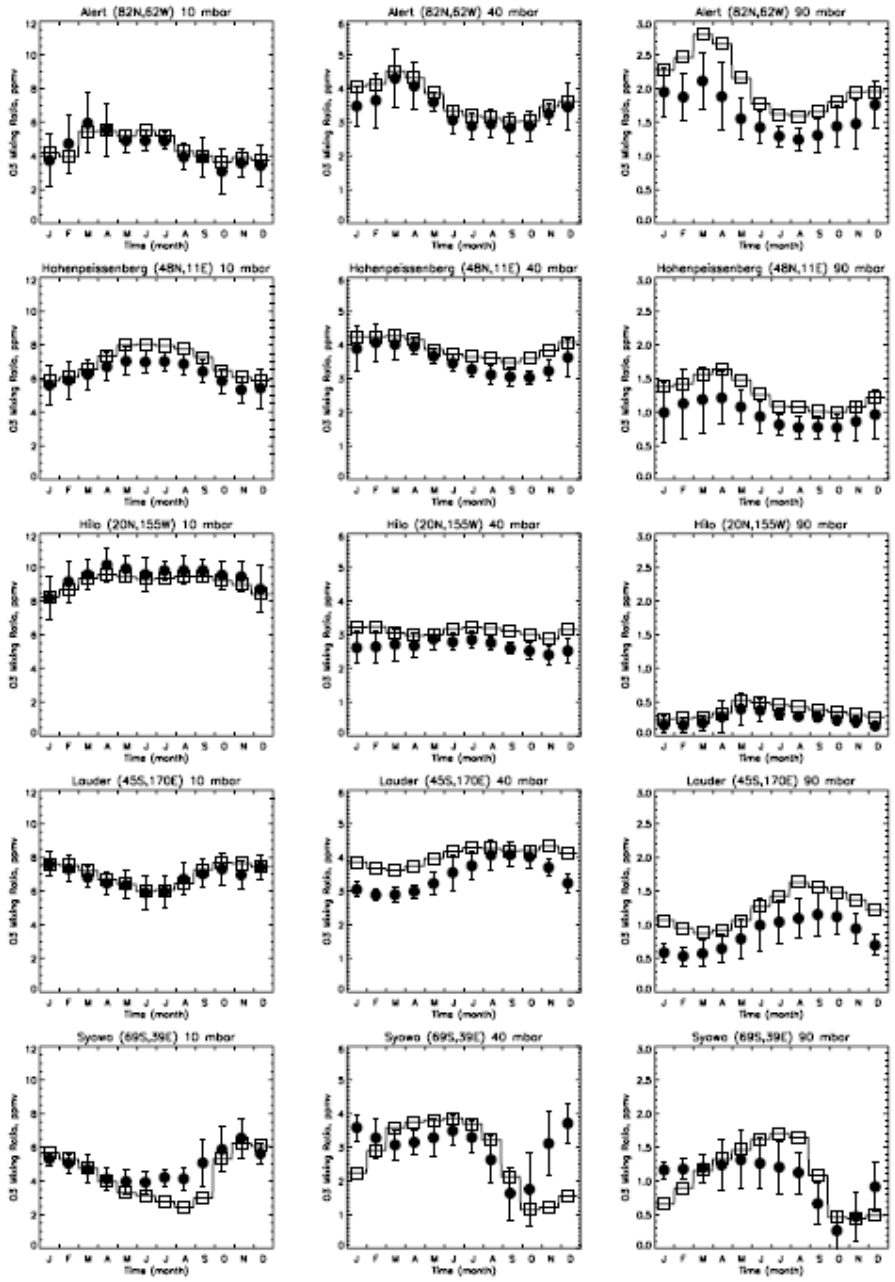

Figure 12: Seasonal variation of O3 mixing ratios (ppmv) over different stations measured by sondes and simulated by the model. Measurements (black dots) and simulated mixing ratios (open squares) are averaged over the period 1986-1995. Note that the standard deviation for the model is not shown as for practical reasons we archived 5-day average outputs for most of the years of simulation.

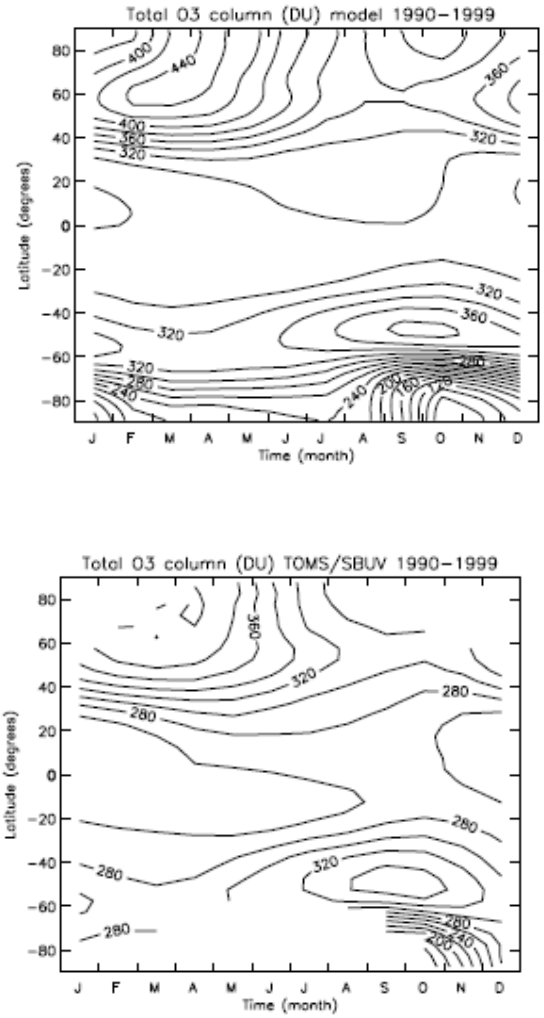

Figure 13: Variation of total ozone (in Dobson unit) with latitude and time (month); top panel: mean value for the last 10 years of the simulation (1990-1999), bottom panel: mean value of TOMS/SBUV observations for the period 1990-1999.

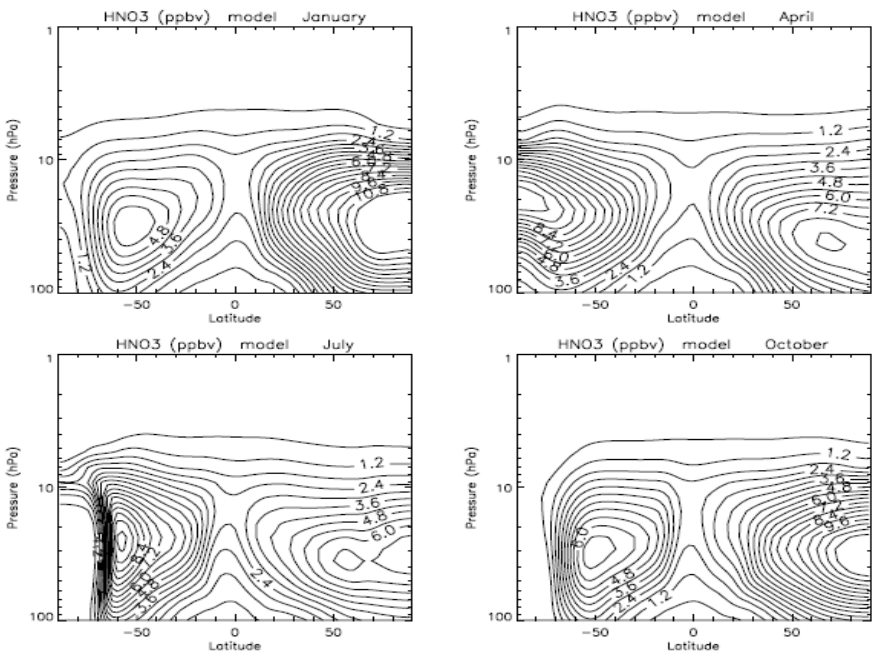

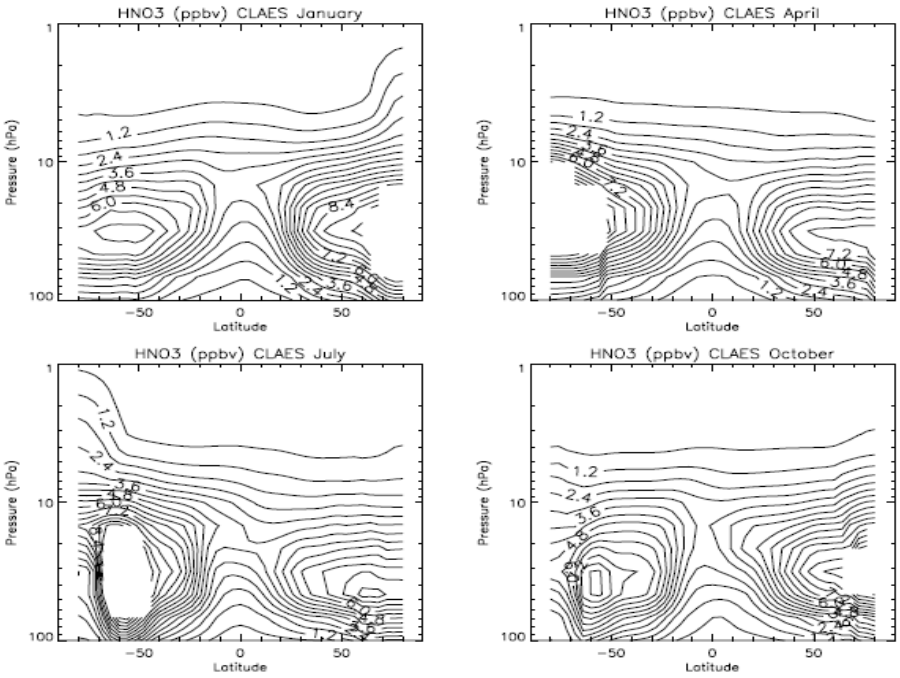

Figure 14: January and July zonal mean distributions of HNO3 mixing ratios (ppbv) simulated by the model for the period 1990-1999 (top) and observed by CLAES (bottom).

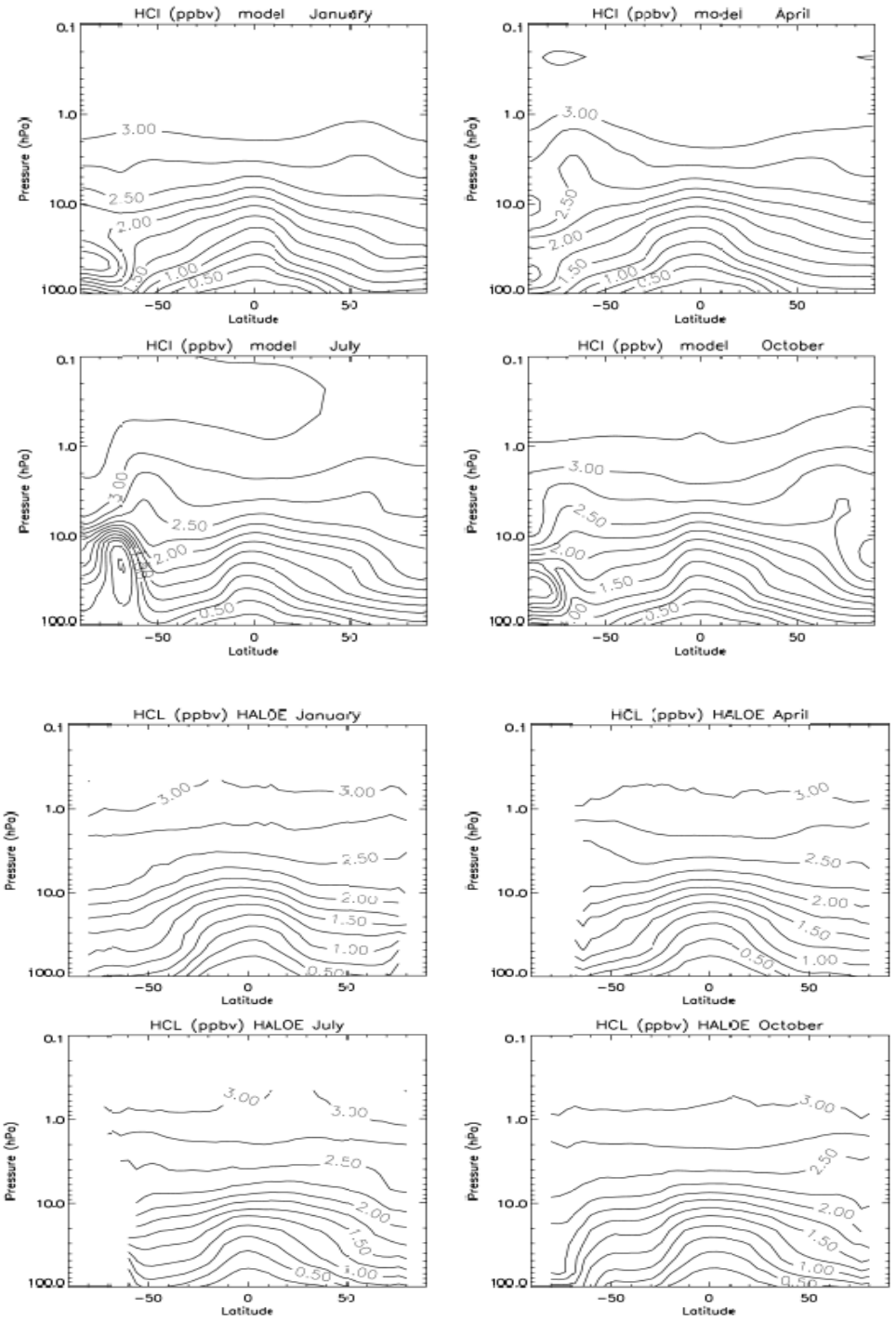

Figure 15: January and July zonal mean distributions of HCL mixing ratios (ppbv) simulated by the model for the period 1990-1999 (top) and observed by HALOE (bottom).

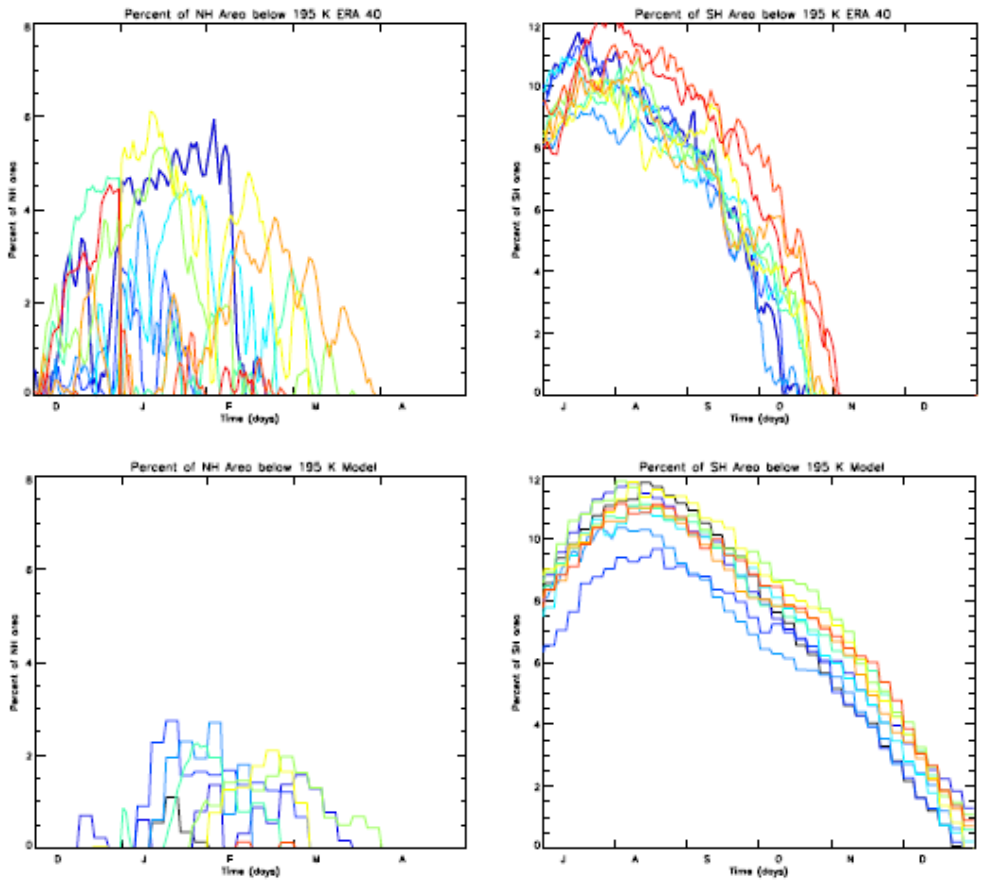

Figure 16: Fractions of the Northern hemisphere area (right) and of the Southern hemisphere (left) covered by PSCs (with temperature below 195 K) at 50 hPa calculated by ERA 40 (top) and simulated by the model (bottom) for the period 1990-1999.

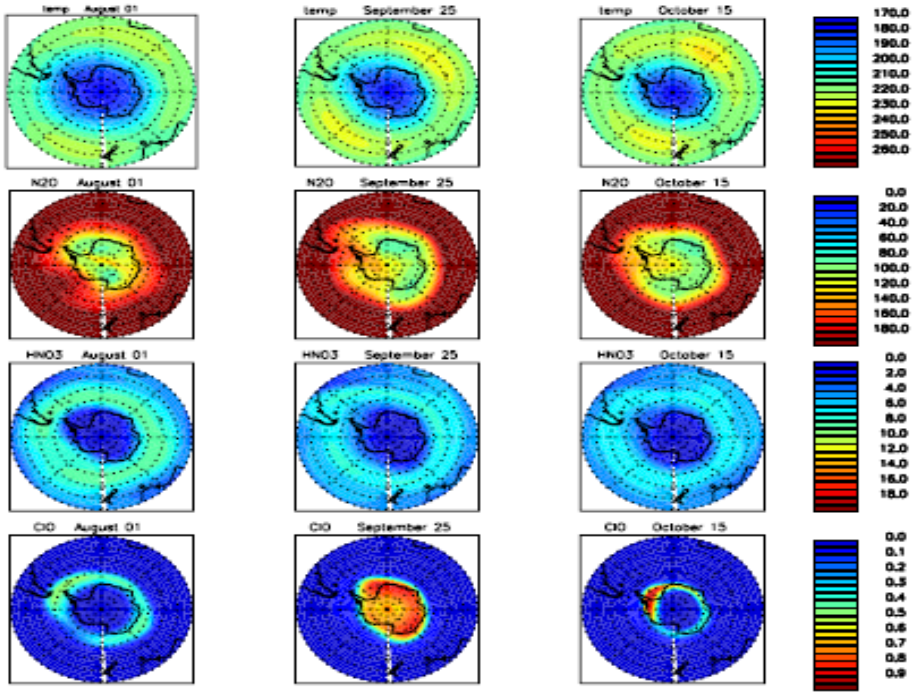

1

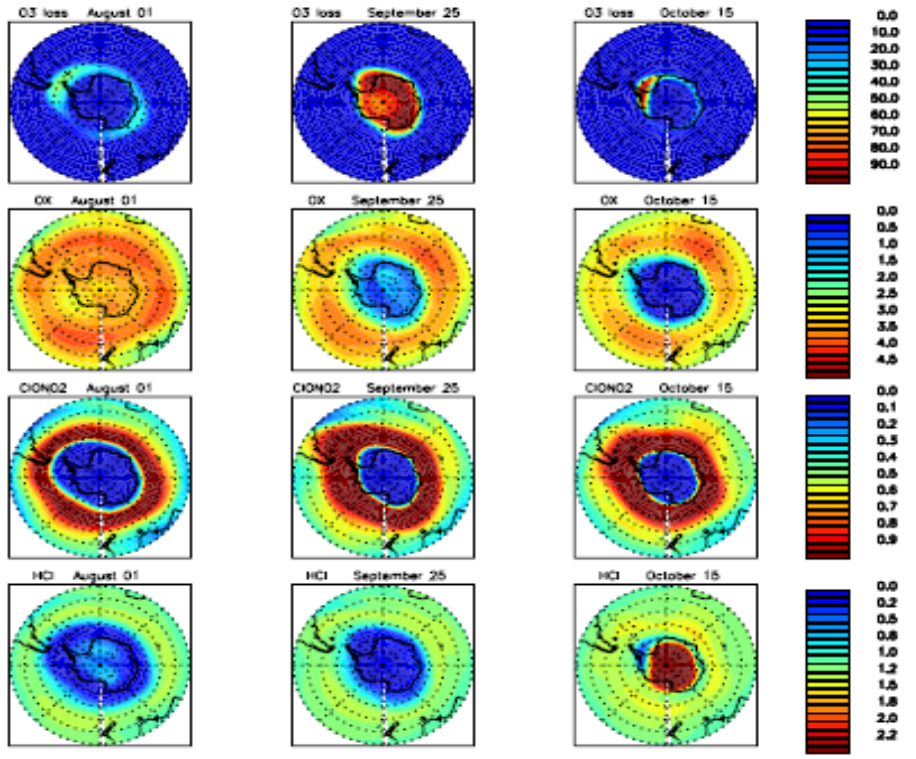

2

3 **Figure 17**: Distribution of the temperature (K), N2O (ppbv), HNO3 (ppbv),
4 ClO (ppbv), chemical loss rate of ozone (ppbv/day), O3 (ppmv), ClONO2

(ppbv), HCl (ppbv) over Antarctic at 50 hPa between late winter and early spring (August 1, September 25, and October 15) for the year corresponding to the 1993 forcing.

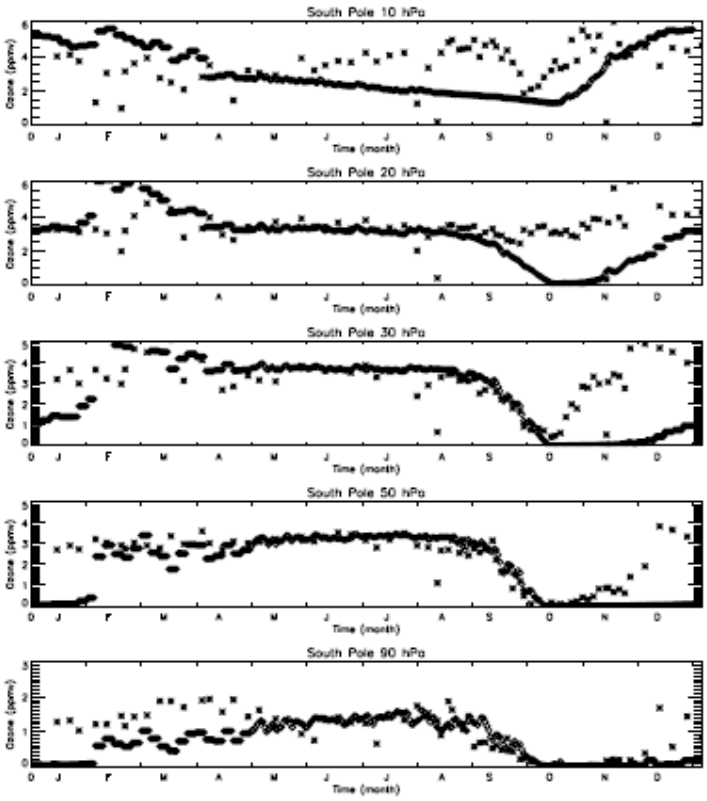

Figure 18: Evolution of the measured (diamonds) and simulated (crosses) ozone mixing ratios at South Pole at 10, 20, 30, 50 and 90 hPa for the year 1993.

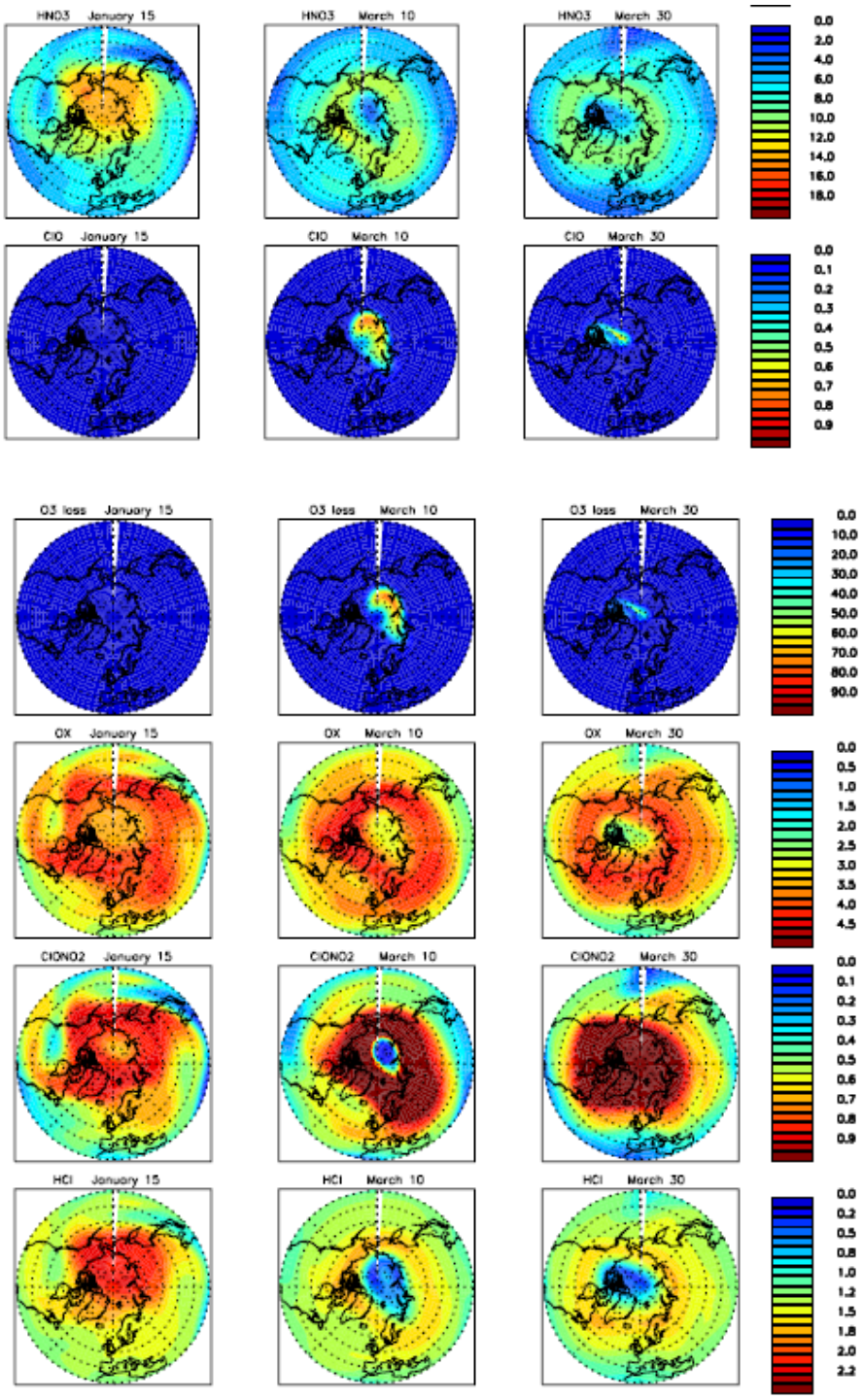

Figure 19: Distribution of HNO3 (ppbv), ClO (ppbv), chemical loss rate of ozone (ppbv/day), O3 (ppmv), ClONO2 (ppbv), HCl (ppbv) over Arctic at 50 hPa between winter and spring (January 15, March 10, and March 30) for the year corresponding to the 1996 forcing.